Ancient TL

www.ancienttl.org · ISSN: 2693-0935

Issue 37(1) - June 2019
https://doi.org/10.26034/la.atl.v37.i1

ISSN 0735-1348

Ancient TL

A periodical devoted to Luminescence and ESR dating

Department of Physics, East Carolina University, 1000 East 5th Street, Greenville, NC 27858, USA
http://ancienttl.org

June 2019, Volume 37 No.1

Ancient TL

Started by the late David Zimmerman in 1977

Ancient TL

How reliable are our beta-source calibrations?

Chantal Tribolo[1*], Sebastian Kreutzer[1], Norbert Mercier[1]

[1] IRAMAT-CRP2A, UMR 5060, CNRS – Université Bordeaux Montaigne, 33607, Pessac Cedex, France

[*]Corresponding Author: ctribolo@u-bordeaux-montaigne.fr

Received: November 29, 2018; in final form: April 18, 2019

Abstract

The calibration of any artificial β-source attached to a luminescence reader is fundamental for the accuracy of luminescence dating results. Here, we present calibration results obtained for a β-source attached to a single grain Risø reader in Bordeaux using a series of quartz of different origins. The quartz was irradiated with three different γ-irradiators. An unexpected variability of the apparent dose rates was observed and our results suggest that the γ-irradiation is the main reason for this variability. Further work is needed to clarify the underlying reasons.

Keywords: Source calibration; luminescence dating; quartz

1. Introduction

The calibration of any artificial β-source commonly attached to a luminescence reader is a fundamental step for applying luminescence dating methods. However, despite its importance for the overall accuracy and comparability of the results obtained across luminescence dating laboratories worldwide, no calibration procedure largely validated and performed by the luminescence community has been agreed on during the last 30 years. As a consequence, each luminescence dating laboratory defines its calibration strategy, although a few studies have drawn attention to difficulties encountered with different materials and to sample specific effects (e.g., optical attenuation), with the measurement procedures and with the physics of β-particles themselves, including build-up and backscattering effects as well as non-uniformity of the dose rate due to field gradients test (e.g., Aitken 1985 and references therein; Bell & Mejdahl 1981; Göksu et al. 1995; Kadereit & Kreutzer 2013; Guérin & Valladas 2014).

In practice, natural materials (e.g., quartz, flint, quartzite pebbles, feldspars, calcite, ...) similar to those dated with the luminescence methods are usually preferred for calibration (e.g., Pernicka & Wagner, 1979), although alternatives based on artificial materials (e.g., Al_2O_3:C, CaF_2) have also been suggested in the past (e.g., Erfurt et al., 2001). Nowadays, quartz appears to be the most commonly dated natural mineral with luminescence methods. Hence, using quartz for β-source calibration appears to be a logical step, providing its luminescence properties are suitable for high-precision calibration work. To date, two types of 'calibration quartz' are commercially available: from the Risø National Laboratory (DTU Nutech) (Hansen et al., 2015, 2018), henceforth named 'Risø calibration quartz' (RCQ), and more recently from Freiberg Instruments GmbH (D. Richter, pers. comm.), henceforth named LexCal2014 quartz (LCQ). In both cases, batch numbers (#) are assigned to distinguish between calibration materials prepared and irradiated at different times.

The RCQ and the LCQ, in conjunction with the single aliquot regenerative (SAR) dose protocol (Murray & Wintle, 2000) provide a convenient way of obtaining dose rate values for many laboratories worldwide. However, and despite of the tests that have been carefully run on these materials before they were shipped to the luminescence community (Hansen et al. 2015; Hansen et al. 2018; D. Richter, pers. comm.), this 'commonly' followed procedure is not free from drawbacks and requires leaps of faith. Underlying premises are: (1) the quartz luminescence signals are stable over time, (2) their test dose response corrections are accurate, (3) those quartz samples have a suitable "average behaviour" (compared to other natural quartz) and (4) they are highly representative. Furthermore, Hansen et al. (2015, 2018) have shown that, for reasons not yet fully understood, the variability of the calibration dose rates obtained using different batches of the RCQ, or within one batch for different periods of measurement, is

much higher than expected: "any calibration can be up to 10% (95% probability) away from the mean" (Hansen et al., 2015).

At the IRAMAT-CRP2A luminescence dating laboratory in Bordeaux, the two commercially available 'calibration quartz' samples are routinely measured for estimating β-sources dose rates by applying SAR OSL. We repeat these tests for each β-source attached to a luminescence reader at least twice a year to verify the dose rates. The average dose rate and the associated uncertainty for a given source are determined from the entire (growing) time series. Additionally, considering the potential limitations of these two materials, quartz originating from various dating studies have also been investigated recently.

In practice, whereas Hansen et al. (2015, 2018) focused on multi-grain measurements and compared different batches of the same quartz or, different quartz (or feldspars) irradiated with the same facility, here we report single grain measurements for all the quartz samples considered here: RCQ, LCQ and quartz samples of different origins that were γ-irradiated with different facilities.

Our contribution does not aim at discarding or favouring a specific calibration material or γ-source but aims at encouraging discussions on this important topic which we believe to be of relevance for the upcoming Trapped Charge Dating Association.

2. Material and Methods

Table 1 summarises the different quartz samples that were used as calibration materials, and which are grouped into three categories according to their provenance. Table 2 summarises central information available in the literature for the employed γ-source facilities and the method used for their calibration. At Munich and Risø, the air kerma is deduced from measurements with an ionisation chamber, calibrated against a primary beam. The air kerma for such a beam is generally known with a high precision (< 0.5%) and the facilities follow ISO standards (for Munich, e.g., Greiter et al. 2016). However, the geometry of the quartz grain container differs as well as the mode of calculation of the dose to quartz (analytic against numeric – Monte Carlo Markov Chain). The γ-facility at the "*Laboratoire des Sciences du Climat et de l'Environnement*" (LSCE, Gif-sur-Yvette, France) is not directly calibrated with an ionization chamber, but calibration results from comparisons of TL signals (for quartzite pebbles) for this beam and a secondary ^{60}Co beam (Table 2).

Group (A). It includes five batches of RCQ (see Hansen et al. 2015, 2018 for details about origin, preparation and characteristics): #40, #90, #106 and #113, plus one batch that was provided in 2013 but was not tagged with a specific batch number; henceforth it will be called "#2013". For four out of the five batches, the granulometric fraction of

Table 1. List of samples with the corresponding SAR parameters. Each dose-response curve was fitted with a single saturating exponential. The stimulation time was 1 s, and the first 0.06 s and last 0.12 s were taken for signal and background respectively.

sample	supplier	geological / archaeological origin	grain size	preheat/cutheat	optical wash	regenerative doses (s) /test doses (s)
RCQ #40	DTU Nutech	sand dune, Rømø, Jutland, South western Denmark (Tindahl Madsen et al., 2007; Hansen et al., 2015)	∼120 µm	260 °C 10 s/ 220 °C 10 s	280 °C 40 s	20,35,45,90,0,20/20
RCQ #90	DTU Nutech		180 – 225 µm	260 °C 10 s/ 220 °C 10 s	280 °C 40 s	20,35,45,90,0,20/20
RCQ #106	DTU Nutech		180 – 225 µm	260 °C 10 s/ 220 °C 10 s	280 °C 40 s	20,35,45,90,0,20/20
RCQ #113	DTU Nutech		180 – 225 µm	260 °C 10 s/ 220 °C 10 s	280 °C 40 s	20,35,45,90,0,20/20
RCQ #2013	DTU Nutech		180 – 225 µm	260 °C 10 s/ 220 °C 10 s	280 °C 40 s	20,35,45,90,0,20/20
LCQ	Freiberg Instruments GmbH	sand dune, Schletau, Germany (Hilgers 2007; Breest et al. 2001; Tolksdorf et al. 2013; Turner et al. 2013; D. Richter, pers. comm.)	∼120 µm	200 °C 10 s/200 °C cut	no	10,20,30,60,0,20/20
SB7	IRAMAT-CRP2A	Sibudu Cave, South Africa	200 – 250 µm	260 °C 10 s/240 °C cut	280 °C 40 s	700,1400,2800,5600,0,700/250
SB12	IRAMAT-CRP2A	Sibudu Cave, South Africa	200 – 250 µm	260 °C 10 s/240 °C cut	280 °C 40 s	300,600,1200,2400,4800,0,300/250
DRS5	IRAMAT-CRP2A	Diepkloof Rock Shelter, South Africa	200 – 250 µm	260 °C 10 s/160 °C cut	no	400,800,1600,3200,0,400/400
DRS9	IRAMAT-CRP2A	Diepkloof Rock Shelter, South Africa	200 – 250 µm	260 °C 10 s/220 °C 10 s	no	400,800,1600,3200,0,400/400
DRS11	IRAMAT-CRP2A	Diepkloof Rock Shelter, South Africa	200 – 250 µm	260 °C 10 s/220 °C 10 s	no	600,1200,2400,4800,0,600/400
BRS2	IRAMAT-CRP2A	Bushman Rock Shelter, South Africa	200 – 250 µm	260 °C 10 s/160 °C cut	no	100,200,400,800,0,100/100
UBB5	IRAMAT-CRP2A	Umbeli Belli, South Africa	200 – 250 µm	260 °C 10 s/220 °C 10 s	no	400,800,1600,3200,0,400/400
UBB6	IRAMAT-CRP2A	Umbeli Belli, South Africa	200 – 250 µm	260 °C 10 s/220 °C 10 s	no	400,800,1600,3200,0,400/400

Table 2. Main characteristics for the γ-irradiation facilities employed in this study and procedure for estimating the given dose.

facility	radioisotope	calibration of the γ-source	dosing of the "calibration" quartz			reference
			packing	geometry of irradiation	calculation of the γ-dose to quartz	
Risø	^{137}Cs	Ionisation chamber measuring air kerma, calibrated at the National Physical Laboratory, United Kingdom. Air kerma known at ± 1%	5 g of loose grains in a planar 100 x 100 x 4.8 mm^3 glass cell (2 mm wall thickness, 1 mm cavity; inner volume 6.5 cm^3) wrapped in black plastic	Irradiation in a beam at a distance of 2 m in a calibrated scatter-free geometry using a point-source of ^{137}Cs	Calculation of the SiO_2 kerma considering the mass-energy absorption coefficients for SiO_2 and air; calculation of the γ-attenuation in the cell and quartz grains volume assuming charge particle equilibrium and exponential attenuation law. Dose absorbed by SiO_2 = calibrated air kerma x (SiO_2 kerma/air kerma) x attenuation	Hansen et al. (2015); Bos et al. (2006); A. Murray., pers. comm.
Munich	^{137}Cs	Ionization chamber, calibrated against the primary standard of the PTB, Germany. Air kerma known at ± 1%	Loose grains in a planar 45 x 12.5 x 12.5 mm^3 glass cell (wall thickness 4.2 and 4.3 mm, 5 mm cavity; inner volume 1.75 cm^3)	Irradiation in a beam at a distance of 1 m from the ^{137}Cs source; the field radiation is not exactly parallel at this location and an additional 1.2% uncertainty is taken into account.	Absorbed dose in quartz per air kerma calculated using the Monte Carlo Code MCNPX 5 (X-5 Monte Carlo Team, 2003). Estimated error of the Monte Carlo approach: 1.4%. The total error on the dose (2.1%) combines (quadratically) with this uncertainty, the uncertainty of the air kerma and the uncertainty due to the geometry of the field.	D. Richter (pers. comm.); Greiter et al. (2016)
LSCE	^{137}Cs	Comparing TL signals (for 12 different crushed quartzite pebbles) after irradiation with a ^{60}Co beam (secondary French National beam) for one set of aliquots and with the LSCE γ-source for another set of aliquots.	60 mg of loose grains in cylindric plastic cells (height: 6 mm)	Six sources of ^{137}Cs are located along a circular ring (diameter 5 cm). The cell containing the grains is located at the center where the vertical flux of γ-rays is homogeneous (< 0.5% variability).	The calibration dose rate of this γ-source is known by comparison of the TL signals of crushed quartzite pebbles obtained after irradiation in a primary source (see column 3).	Valladas (1978); Mercier et al. (2012)

the quartz grains is 180 – 250 μm, but it is much smaller (about 120 μm) for batch #40. For batch #106, both the unirradiated and γ-irradiated (4.81 ± 0.14 Gy) fractions were available whereas batches #40, #113, and #2013 were limited to the irradiated fraction (4.81 ± 0.14 Gy). For #90, only the 0 Gy (zero dose) fraction was usable, since the 4.81 Gy fraction had been exhausted for calibrating other equipment. This fraction received a dose of 5 Gy (±3%) using the γ-source facility of the LSCE (Valladas, 1978).

Group (B). This group consists of the first batch of the LCQ provided by Freiberg Instruments GmbH (D. Richter, pers. comm.). Two subsamples are available: one had been irradiated (3.00 ± 0.06 Gy) with a ^{137}Cs γ-source "Buchler Gammakalibrator OB 20" at the IAEA/WHO Secondary Standard Dosimetry Laboratory (SSDL) of the Helmholtz Zentrum München (D. Richter, pers. comm.); facility: Greiter et al. 2016) (henceforth termed 'Munich') and a second subsample, not dosed, was also provided.

Group (C). This group combines eight different quartz samples originating from four South African prehistoric sites: Sibudu (SB7 and SB12), Bushman Rock Shelter (BRS2), Umbeli Belli (UBB5 and UBB6), and Diepkloof Rock Shelter (DRS5, DRS9 and DRS11) (e.g., Tribolo et al., 2013; Soriano et al., 2015; Porraz et al., 2018; Bader et al., 2018). All these samples have been naturally bleached during the Middle Stone Age period and have then received potentially measurable equivalent doses. Except for Sibudu and Umbeli Belli, which are distant from each other only by few tens of kilometres, the sites are separated by more than 1,000 km. We therefore consider those quartz samples as being of different origins. They are all bright and their OSL signal is dominated by a fast component (checked with LM-OSL (Bulur, 1996) measurements and compared to the RCQ). For all of them, the 200 – 250 μm granulometric fraction was available. The quartz samples were bleached twice for one minute in a Hönle SOL500 solar simulator with, at least, a pause of three hours between the two bleaching steps. Each bleached sample was divided into two subgroups: one was kept unirradiated and the other part was sent to the LSCE for γ-irradiation. For calibrating our β-source, we administered large doses between 30 Gy and 180 Gy (± 3%), which were chosen to be similar in size to natural doses.

All quartz samples were mounted on single grain (SG) discs facilitating 100 holes (theoretical diameter: 300 μm; depth: 300 μm). All these discs are supposed to be identical; however, they differ for several reasons: (1) SG discs tend to become worn out over time, i.e. the coating degrades and eventually falls apart. (2) Different batches of discs bought at different times do not have precisely the same characteristics, e.g., the diameters and depth of the holes are larger for some batches (closer to 350 μm) than for the other batches. To test the influence of the disc condition and geometry on the apparent calibration dose rate we measured one material (RCQ, #113) with different sets of discs: new, old with small holes, and almost new with large holes.

All measurements were performed on a single machine (and with a single carrousel): a Risø TL-OSL DA-20 single grain reader (basic design: Bøtter-Jensen et al. 2000). A 10 mW Nd:YVO_4 diode-pumped green laser (532 nm) was used for stimulation and the luminescence signal was detected with a PDM9107-CP-TTL photomultiplier tube through a combination of Hoya U340 glass filters (3 x 2.5 mm). The β-source ^{90}Sr/^{90}Y attached to this reader has a nominal activity of 1.2 GBq. The irradiation field of this source revealed a non-uniformity that needs to be corrected and taken into account for the data analysis. To perform the correction, we used the software '*CorrSGbin*' provided by DTU Nutech (Lapp et al., 2012). However, in our experiments, we found that the mean dose rate appeared to be unaffected by this correction (data not shown).

Before starting the calibration measurements, the efficiency of the SAR protocol was systematically checked: a β-dose was given by the source attached to the reader to the unirradiated fractions (i.e. RCQ #106, LCQ, all the South African quartz). When no unirradiated fraction was available (for the RCQ batches #40, #113 and #2013), the zero dose quartz of RCQ#106 was analysed, assuming that all the RCQ batches would support the same protocol on the same machine; a behaviour confirmed by our time series calibrations. For each measured aliquot, the normalized (L_x/T_x) OSL signals were fitted with a saturating exponential: $L_x/T_x = a * (1 - exp^{-(b+D)/D_0})$, where D is the regenerative dose and a, b and D_0 are fitting parameters. Table 1 summarises the parameters (preheat temperatures) and measurements conditions (regenerative doses) applied for each sample.

A series of rejection criteria were used for the grain selection: (1) natural test dose signal at least 3 times above background, (2) natural test dose relative error < 10%, and (3) recuperation < 5% of the natural signal. Note that, according to our own observations, the recycling ratio seems not to be a key criterion as already suggested by, e.g., Guérin et al. (2015) and Thomsen et al. (2016), and was thus not used as a selection criterion. In addition, since for some of our quartz samples the given dose is high (up to 180 Gy) and may, therefore, induce signal saturation problems for some of the grains, an additional criterion was applied based on the saturation parameter D_0 (cf. Thomsen et al., 2016).

For each series of measurements, the central dose model (Galbraith et al., 1999) was applied for calculating the final dose and hence, the apparent dose rate of our β-source.

The software *Analyst* (v4.52; Duller 2015) was used for the data analyses. Plots were produced using the **R** (R Core Team, 2018) package `'Luminescence'` (Kreutzer et al., 2012, 2018).

Table 3. Dose recovery ratio and calibration dose rates obtained for the different samples. We used the adjectives "old" to describe SG discs that were somewhat worn out, "new" to label so far untouched discs and "large" to label discs with holes that are larger than they are for the "new" and "old disc" (see main text). The γ-doses have associated relative uncertainties at one sigma of 3% for the LSCE and Risø facilities and 2% for the Munich facility. Where indicated, the dose recovery tests were performed with the unirradiated part of the sample just before the calibration measurements. The [x] symbol indicates that the test was performed just before the calibration measurement, but on the 0 Gy RCQ fraction of #106. The calibrations were performed over several months but for comparison, all the dose rates are re-calculated for 2018-10-25. n/N indicates the number of accepted over the number of measured grains (1) for the dose recovery tests, (2) for the calibration measurements. The sensitivity change is based on the "test-signal-change" calculated in Analyst, corresponding to the ratio between the last and first test dose signal.

sample	disc	given γ-dose (Gy)	γ-source	date of measure-ment	dose recovery tests				dose rate measurements			
					n/N (1)	dose recovery ratio	OD (%)	sensitivity change	n/N (2)	calculated dose rate on 2018-10-25	OD (%)	sensitivity change
RCQ#106	old	4.81	Risø	Jan-17	265/400	1.06 ± 0.01	9 ± 1	0.8 ± 0.2	254/400	0.106 ± 0.002	12 ± 1	0.9 ± 0.2
RCQ#106	old	4.81	Risø	Jul-17	257/400	1.00 ± 0.01	5 ± 1	0.8 ± 0.2	319/400	0.105 ± 0.002	17 ± 1	0.9 ± 0.2
RCQ#106	old	4.81	Risø	Sep-17	298/400	1.11 ± 0.01	22 ± 1	0.8 ± 0.2	339/400	0.104 ± 0.002	12 ± 1	0.9 ± 0.2
RCQ#2013	new	4.81	Risø	May-18	256/400	[x]1.02 ± 0.01	7 ± 1	0.8 ± 0.2	202/800	0.123 ± 0.002	13 ± 1	4.1 ± 3.2
DRS9	old	100	LSCE	May-18		nd			71/1700	0.127 ± 0.002	10 ± 2	1.1 ± 0.3
RCQ#113	new	4.81	Risø	May-18	271/400	[x]1.00 ± 0.00	0	0.8 ± 0.2	255/400	0.104 ± 0.002	19 ± 1	1.1 ± 0.3
RCQ#113	old	4.81	Risø	May-18		nd			279/400	0.108 ± 0.002	10 ± 1	1.2 ± 0.3
RCQ#113	new	4.81	Risø	May-18		nd			256/400	0.106 ± 0.002	10 ± 1	1.1 ± 0.3
RCQ#113	large	4.81	Risø	May-18		nd			289/400	0.104 ± 0.002	0	1.1 ± 0.2
LCQ	old	3	Munich	May-18		nd			65/300	0.127 ± 0.004	11 ± 2	0.7 ± 0.2
DRS9	old	100	LSCE	May-18	70/800	1.03 ± 0.02	12 ± 2	1.1 ± 0.3	64/1100	0.126 ± 0.003	10 ± 2	1.1 ± 0.3
DRS11	old	100	LSCE	May-18	26/800	0.96 ± 0.01	16 ± 2	1.2 ± 0.3	26/500	0.117 ± 0.003	9 ± 2	1.2 ± 0.3
DRS5	old	100	LSCE	Jun-18	47/700	1.01 ± 0.02	9 ± 2	1.4 ± 0.5	27/700	0.111 ± 0.005	18 ± 4	1.5 ± 0.5
RCQ#90	old	5	LSCE	Sep-18		nd			316/400	0.122 ± 0.001	10 ± 1	1.0 ± 0.2
RCQ#113	old	4.81	Risø	Sep-18		nd			262/400	0.111 ± 0.001	9 ± 1	1.2 ± 0.3
BRS2	old	30	LSCE	Sep-18	201/300	1.03 ± 0.01	10 ± 1	1.1 ± 0.3	335/500	0.120 ± 0.004	11 ± 1	1.2 ± 0.4
SB12	old	80	LSCE	Sep-18	85/300	1.03 ± 0.02	15 ± 2	1.0 ± 0.34	83/300	0.124 ± 0.003	15 ± 2	0.9 ± 0.3
UBB5	old	45	LSCE	Sep-18	143/500	0.95 ± 0.01	12 ± 0	1.3 ± 0.4	165/500	0.126 ± 0.004	14 ± 1	1.3 ± 0.4
UBB6	old	100	LSCE	Sep-18	58/700	1.00 ± 0.02	12 ± 3	1.0 ± 0.2	43/700	0.124 ± 0.005	14 ± 3	1.0 ± 0.2
SB7	old	180	LSCE	Oct-18	24/600	1.03 ± 0.04	12 ± 3	0.8 ± 0.2	50/600	0.114 ± 0.005	16 ± 2	0.8 ± 0.2
RCQ#113	old	4.81	Risø	Sep-18	227/400	[x]1.00 ± 0.01	2 ± 1	0.8 ± 0.2	262/400	0.109 ± 0.001	10 ± 1	1.2 ± 0.4
RCQ#2013	old	4.81	Risø	Sep-18		nd			99/400	0.117 ± 0.002	12 ± 1	3.3 ± 1.6
RCQ#40	old	4.81	Risø	Sep-18		nd			30/400	0.111 ± 0.003	10 ± 2	0.7 ± 0.2
LCQ	old	3	Munich	Oct-18	108/600	1.00 ± 0.01	7 ± 2	0.8 ± 0.2	98/600	0.125 ± 0.003	15 ± 2	0.8 ± 0.2

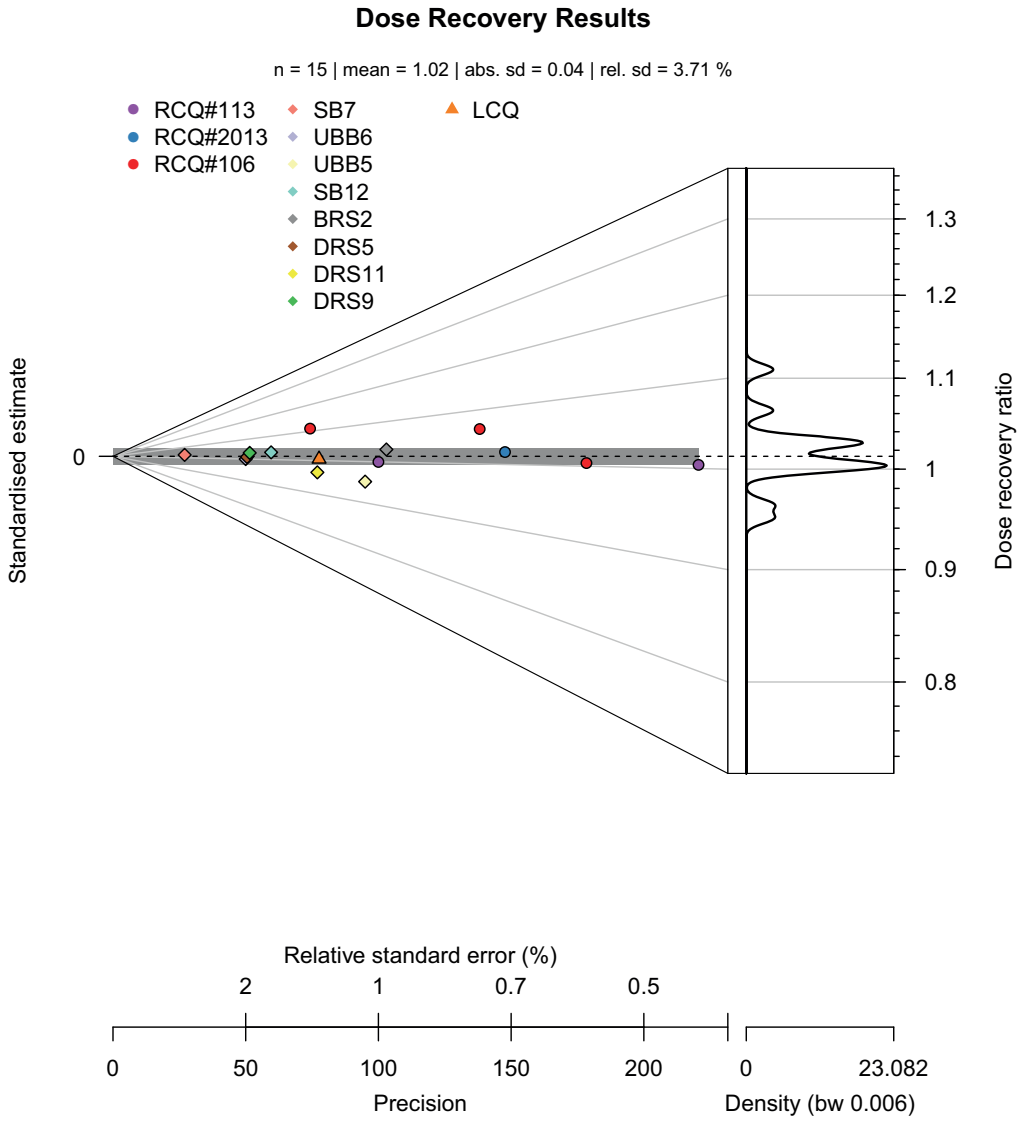

Figure 1. Abanico plot (Dietze et al., 2016) of the dose recovery ratio. Different samples are colour coded. Circles display samples irradiated at Risø; rectangle show samples irradiated at the LSCE; triangles are used for samples irradiated at Munich.

3. Results

Results are presented in Table 3 and in Figures 1 and 2. Except for one case (RCQ#106 from September 2017), the dose recovery ratios are consistent with unity or within 5% of unity. The central[1] ratio for all the data is 1.02 ± 0.01 with an overdispersion (OD) of $3 \pm 1\%$ (Fig. 1).

The apparent dose rates deduced from the calibration measurements show a significant dispersion (0.115 ± 0.002 Gy/s, OD $7 \pm 1\%$). Two dose rate groups can be distinguished: the first includes the LCQ (irradiated in Munich), all the South African quartz samples and the RCQ #90 irradiated at the LSCE, as well as the RCQ #2013 (irradiated at DTU Nutech) (central dose: 0.122 ± 0.001 Gy/s, OD: $2 \pm 1\%$). The second group includes the RCQ #113, #40 and #106 and potentially, two south African quartz samples having a lower precision (SB7 and DRS5) (central dose: 0.107 ± 0.001 Gy/s, OD: $2 \pm 1\%$). The 14% difference between the central dose values for these two groups is statistically significant (two-sided paired *t-test,* p-value: < 0.01).

Note 1: Additionally, we have performed a few multiple grain measurements on other readers with similar results. To keep the text concise, only the SG measurements for one reader are reported.

Note 2: The 12% discrepancy between one of the RCQ (#2013) alone and the other RCQ (#40, #106, #113) is consistent with those reported by Hansen et al. (2015, 2018).

[1] In all the data presented here, the differences between the arithmetic mean and the central dose rates following Galbraith et al. (1999) are negligible.

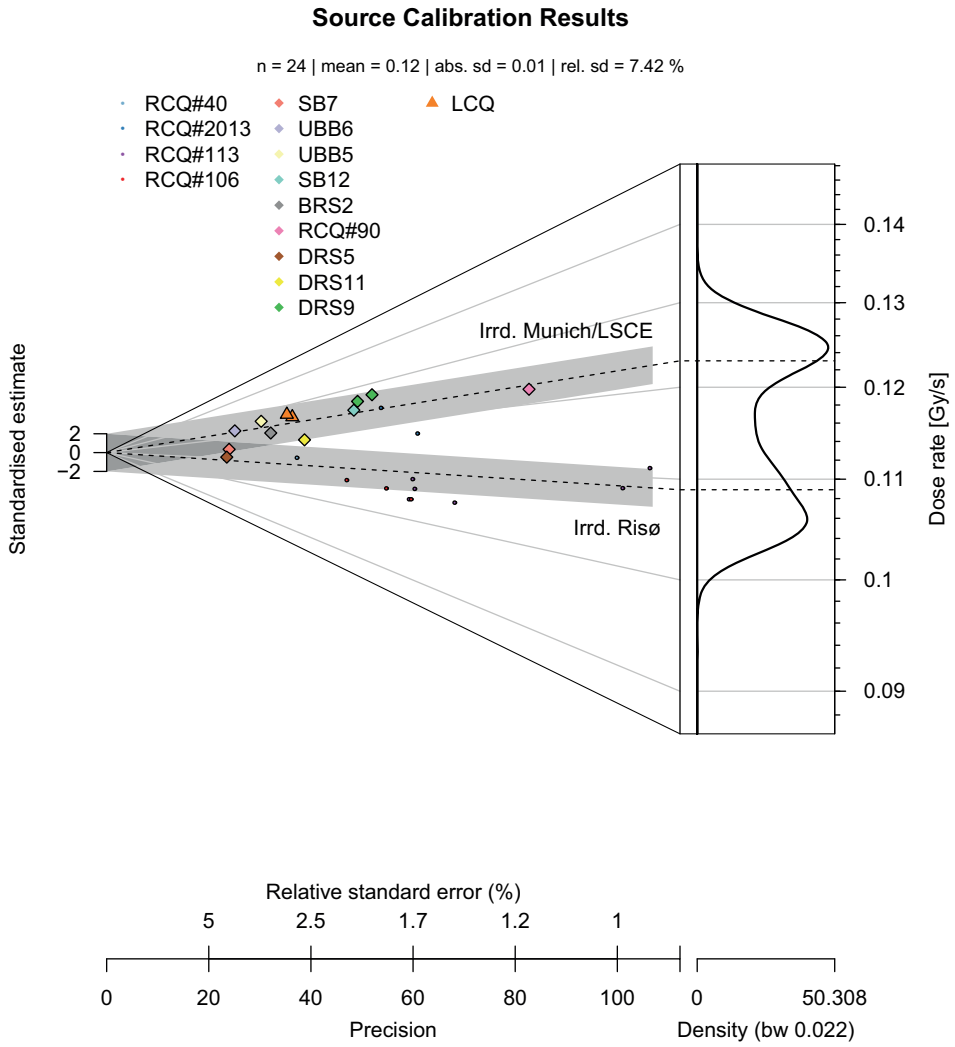

Figure 2. Abanico plot (Dietze et al., 2016) of the obtained calibration dose rates. Different samples are colour coded (similar to Fig. 1). Circles display samples irradiated at Risø; rectangles show samples irradiated at the LSCE; triangles are used for samples irradiated at Munich.

4. Discussion

The mean sensitivity changes vary for all samples except for RCQ#2013, between 0.7 ± 0.2 and 1.5 ± 0.5 (ratio of last and first test dose signal; Table 3). As expected, they are similar for the non-irradiated and the corresponding γ-irradiated samples. This is unfortunately not true for RCQ#2013 whose mean sensitivity changes are significantly higher (4.1 ± 3.2 and 3.3 ± 1.6). This weakens the use as a surrogate for dose recovery test of RCQ#106 and might explain partly why this RCQ quartz gives an apparent dose rate significantly different from the other RCQ. Except for RCQ#2013, we did not observe correlations between the sensitivity changes and the apparent dose rates (data not shown).

The consistency of the dose recovery ratio with unity and the low OD observed there ($3 \pm 1\%$, compared to the $2 \pm 1\%$ observed for each calibration group) suggests that neither the protocol nor the stability of the equipment is responsible for the observed differences between the calibration dose rates. The $2 \pm 1\%$ OD for each group may reflect small "behavioural" differences between the quartz samples.

The software *CorrSGbin* (Lapp et al., 2012) was applied to the data before the analyses to correct for the non-uniformity of the β-radiation field of the source. Besides, the grains that are selected for the apparent dose rate calculations are sufficiently numerous and well spread over the discs, so that any remaining effect of non-uniformity unlikely caused the observed discrepancy. Figure 3 illustrates our assumption for two examples: RCQ#113 irradiated with the Risø γ-source, and RCQ#90 irradiated in LSCE. All the positions are covered and for a large majority of them, the apparent dose rates of the RCQ#90 are larger than the apparent dose rates of the RCQ#113.

For the first group of calibration dose rates, the consis-

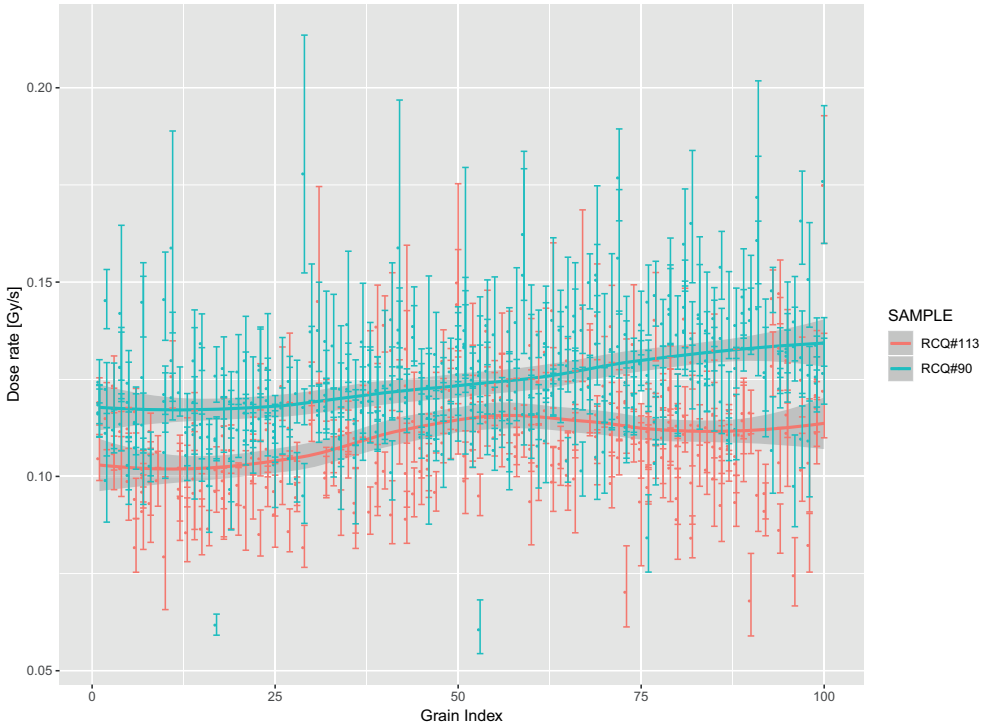

Figure 3. Plot of the apparent dose rate as a function of the grain position on the disc (numbered from 1 to 100). Red dots: RCQ#113, irradiated 4.81 Gy at Risø; turquoise dots: RCQ#90 irradiated with 5 Gy at Gif-sur-Yvette. Error bars represent the individual standard error of each value. While the dose rates between the two batches differ significantly, the variation between the grain positions appears to be random, with a very small increase towards grain position 100.

tency of the results suggests that neither the provenance of the quartz (see also Hansen et al. 2018) nor the value of the artificially given dose (and potential saturation problems) is responsible for the observed discrepancy. For the second group of calibration dose rates which includes #40 (smaller diameter of quartz grains, implying more than one grain per hole) and all the measurements made with different types/qualities of SG discs (#113), we deduce that neither the grain size (ca. 100 µm vs ca. 200 µm), nor the condition of the SG discs is responsible for the observed variability.

Consequently, according to our measurements and observations, it seems that the primary source for the discrepancy between the two groups of apparent dose rates is the γ-dose delivered by the three irradiation facilities.

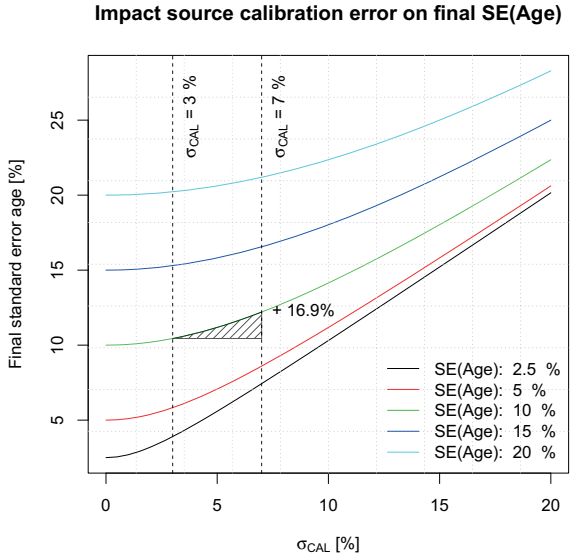

Figure 4. Isoline plots showing the impact of the uncertainty on the calibration dose rate on the final standard error on the age, for various values of $\sqrt{\left(\left(\frac{\sigma_D}{D}\right)^2+\left(\frac{\sigma_{D_e}}{D_e}\right)^2\right)}$

For most dating applications, a discrepancy of 14% between two estimates of calibration dose rates is hardly acceptable since a similar offset would be observed in resulting luminescence ages and such value is larger than the average age uncertainties of ca. 9% usually reported ($Q_{0.25}$: 6.8%, $Q_{0.75}$: 12.7%, n_{valid} = 3,484; source: INQUA Dune Atlas, Lancaster et al. 2015). Nonetheless, based on the results presented here, it appears that the current systematic uncertainty of 2% to 4% for the calibration dose rate usually reported might be underestimated.

Since the standard error (SE) of the source calibration impacts all individual doses similarly measured with one reader, it may be considered as a systematic error (cf. Aitken, 1985). To obtain the final standard error for a luminescence age, the following equation can be used:

$$\left(\frac{\sigma_A}{A}\right)^2 = \left(\frac{\sigma_{\dot{D}}}{\dot{D}}\right)^2 + \left(\frac{\sigma_{D_e}}{D_e}\right)^2 + \left(\frac{\sigma_{D_{\mathrm{CAL}}}}{D_{\mathrm{CAL}}}\right)^2$$

where σ_A is the total absolute uncertainty of the age A, ${\sigma_{\dot{D}}}^2$ is the quadratic sum of the absolute systematic and statistical uncertainties of the environmental dose rate $\dot{D}$, σ^2_{De} is the quadratic absolute uncertainty of the equivalent dose D_{e}, and σ^2_{CAL} is the quadratic systematic absolute uncertainty on the calibration dose rate D_{cal}. Figure 4 displays plots of $\frac{\sigma_A}{A}$ as function of $\frac{\sigma_{D_{\mathrm{CAL}}}}{D_{\mathrm{CAL}}}$ for various values of $\sqrt{\left(\left(\frac{\sigma_{\dot{D}}}{\dot{D}}\right)^2 + \left(\frac{\sigma_{D_e}}{D_e}\right)^2\right)}$ (termed SE(Age) in Fig. 4), from 2.5% to 20%. For example, if this quantity is 10% and the relative uncertainty of the calibration dose rate, $\frac{\sigma_{\mathrm{CAL}}}{\mathrm{Dcal}}$, is 7% instead of 3%, it would imply an increase of the coefficient of variation on the age of ca. 17%, from 10.4% to 12.2%. Whether this is acceptable or not depends on the chronological context. Nonetheless, contrary to the various factors used in the age equation for which the uncertainty is both difficult to evaluate precisely, and/or difficult to reduce (water contents, dosimetric heterogeneity, long-term luminescence signal behaviour issues etc.), it seems that the uncertainty of the calibration dose rate could be improved and properly handled.

5. Conclusion

By using a series of different quartz samples ('calibration' quartz commercially available and quartz samples prepared at the IRAMAT-CRP2A), we performed SAR OSL measurements that aimed at determining apparent dose rates for one of our in-built β-source. High variability was observed, and our experiments lead us to conclude that the doses delivered by different irradiation facilities might not be comparable (two groups with a different apparent dose rate of ca. 14%). As a consequence, our observations, in conjunction with those already reported by Hansen et al. (2015, 2018), suggest that the systematic error of 2% to 4% for the calibration dose rate usually reported by the luminescence dating community in dating studies might be underestimated. The source of the observed discrepancy needs to be further investigated. At the IRAMAT-CRP2A, we will continue our investigations with samples irradiated by more than the three here already compared γ-irradiators.

Acknowledgments

The work was supported by the LaScArBx. LaScArBx is a research programme supported by the ANR (ANR-10-LABX-52). It was also funded by the Conseil Regional Nouvelle Aquitaine (project DAPRES_LA_FEM) and the ANR (project DOM-ART n° ANR-16-CE27-0004-01). We are grateful to Hélène Valladas who performed the γ-irradiation at the LSCE. Thanks to Daniel Richter for sharing information on the LexCal quartz and for discussions. David Sanderson provided a very constructive review.

References

Aitken, M. J. *Thermoluminescence dating*. Studies in archaeological science. Academic Press, 1985.

Bader, G. D., Tribolo, C., and Conard, N. J. *A return to Umbeli Belli: New insights of recent excavations and implications for the final MSA of eastern South Africa*. Journal of Archaeological Science: Reports, 21: 733–757, 2018. doi: 10.1016/j.jasrep.2018.08.043.

Bell, W. T. and Mejdahl, V. *Beta Source Calibration and Its Dependency on Grain Transparency*. Archaeometry, 23(2): 231–240, 1981. doi: 10.1111/j.1475-4754.1981.tb00310.x.

Bos, A. J. J., Wallinga, J., Johns, C., Abellon, R. D., Brouwer, J. C., Schaart, D. R., and Murray, A. S. *Accurate calibration of a laboratory beta particle dose rate for dating purposes*. Radiation Measurements, 41(7-8): 1020–1025, 2006. doi: 10.1016/j.radmeas.2006.04.003.

Bøtter-Jensen, L., Bulur, E., Duller, G. A. T., and Murray, A. S. *Advances in luminescence instrument systems*. Radiation Measurements, 32(5-6): 523–528, 2000. doi: 10.1016/S1350-4487(00)00039-1.

Breest, K., Veil, S., Heinemann, B., Hilgers, A., and Willerding, U. *Die Ausgrabungen auf dem mesolithischen Dünenfundplatz Schletau 2000, Ldkr. Lüchow-Dannenberg*. Die Kunde N F, 52: 239–254, 2001.

Bulur, E. *An Alternative Technique For Optically Stimulated Luminescence (OSL) Experiment*. Radiation Measurements, 26(5): 701–709, 1996. doi: 10.1016/S1350-4487(97)82884-3.

Dietze, M., Kreutzer, S., Burow, C., Fuchs, M. C., Fischer, M., and Schmidt, C. *The abanico plot: visualising chronometric data with individual standard errors*. Quaternary Geochronology, 31: 12–18, 2016. doi: 10.1016/j.quageo.2015.09.003.

Duller, G. A. T. *The Analyst software package for luminescence data: overview and recent improvements* . Ancient TL, 33 (1): 35–42, 2015. URL http://ancienttl.org/ATL_33-1_2015/ATL_33-1_Duller_p35-42.pdf.

Erfurt, G., Krbetschek, M. R., Trautmann, T., and Stolz, W. *Radioluminescence (RL) probe dosimetry using Al2O3:C for precise calibration of beta sources applied to luminescence dating*. Radiation Physics and Chemistry, 61(3–6): 721–722, 2001. doi: 10.1016/S0969-806X(01)00386-3.

Galbraith, R. F., Roberts, R. G., Laslett, G. M., Yoshida, H., and Olley, J. M. *Optical dating of single and multiple grains of Quartz from Jinmium Rock Shelter, Northern Australia: Part I, Experimental design and statistical models*. Archaeometry, 41(2): 339–364, 1999. doi: 10.1111/j.1475-4754.1999.tb00987.x.

Göksu, H. Y., Bailiff, I. K., Bøtter-Jensen, L., Brodski, L., Hütt, G., and Stoneham, D. *Interlaboratory beta source calibration using TL and OSL on natural quartz.* Radiation Measurements, 24(4): 479–483, 1995.

Greiter, M. B., Denk, J., and Hoedlmoser, H. *Secondary Standard Calibration, Measurement and Irradiation Capabilities of the Individual Monitoring Service at the Helmholtz Zentrum München: Aspects of Uncertainty and Automation*. Radiation Protection Dosimetry, 170(1-4): 103–107, 2016. doi: 10.1093/rpd/ncv537.

Guérin, G. and Valladas, H. *Cross-calibration between beta and gamma sources using quartz OSL: Consequences of the use of the SAR protocol in optical dating*. Radiation Measurements, 68 (c): 31–37, 2014. doi: 10.1016/j.radmeas.2014.06.010.

Guérin, G., Frouin, M., Talamo, S., Aldeias, V., Bruxelles, L., Chiotti, L., Dibble, H. L., Goldberg, P., Hublin, J.-J., Jain, M., Lahaye, C., Madelaine, S., Maureille, B., McPherron, S. J. P., Mercier, N., Murray, A. S., Sandgathe, D., Steele, T. E., Thomsen, K. J., and Turq, A. *A multi-method luminescence dating of the Palaeolithic sequence of La Ferrassie based on new excavations adjacent to the La Ferrassie 1 and 2 skeletons*. Journal of Archaeological Science, 58(C): 147–166, 2015. doi: 10.1016/j.jas.2015.01.019.

Hansen, V., Murray, A., Buylaert, J.-P., Yeo, E.-Y., and Thomsen, K. *A new irradiated quartz for beta source calibration*. Radiation Measurements, 81: 123–127, 2015. doi: 10.1016/j.radmeas.2015.02.017.

Hansen, V., Murray, A., Thomsen, K., Jain, M., Autzen, M., and Buylaert, J.-P. *Towards the origins of over-dispersion in beta source calibration*. Radiation Measurements, pp. 1–6, 2018. doi: 10.1016/j.radmeas.2018.05.014.

Hilgers, A. *The chronology of Late Glacial and Holocene dune development in the northern Central European lowland reconstructed by optically stimulated luminescence (OSL) dating*. PhD thesis, 2007.

Kadereit, A. and Kreutzer, S. *Risø calibration quartz – a challenge for β-source calibration. An applied study with relevance for luminescence dating*. Measurement, 46(7): 2238–2250, 2013. doi: 10.1016/j.measurement.2013.03.005.

Kreutzer, S., Dietze, M., Burow, C., Fuchs, M. C., Schmidt, C., Fischer, M., and Friedrich, J. *Luminescence: Comprehensive Luminescence Dating Data Analysis*. CRAN, version 0.8.6, 2018. URL https://CRAN.R-project.org/package=Luminescence.

Kreutzer, S., Schmidt, C., Fuchs, M. C., Dietze, M., Fischer, M., and Fuchs, M. *Introducing an R package for luminescence dating analysis*. Ancient TL, 30(1): 1–8, 2012. URL http://ancienttl.org/ATL_30-1_2012/ATL_30-1_Kreutzer_p1-8.pdf.

Lancaster, N., Wolfe, S., Thomas, D., Bristow, C., Bubenzer, O., Burrough, S., Duller, G., Halfen, A., Hesse, P., Roskin, J., Singhvi, A., Tsoar, H., Tripaldi, A., Yang, X., and Zárate, M. *The INQUA Dunes Atlas chronologic database*. Quaternary International, 410: 3–10, 2015. doi: 10.1016/j.quaint.2015.10.044.

Lapp, T., Jain, M., Thomsen, K. J., Murray, A. S., and Buylaert, J. P. *New luminescence measurement facilities in retrospective dosimetry*. Radiation Measurements, 47: 803–808, 2012. doi: 10.1016/j.radmeas.2012.02.006.

Mercier, N., Tribolo, C., Lahaye, C., and Hernandez, M. *Beta-source calibration with quartz: can we determine a single dose-rate?* In *Asia Pacific LED*, volume unpublisherd poster presentation, Japan, 2012.

Murray, A. S. and Wintle, A. G. *Luminescence dating of quartz using an improved single-aliquot regenerative-dose protocol*. Radiation Measurements, 32(1): 57–73, 2000. doi: 10.1016/S1350-4487(99)00253-X.

Pernicka, E. and Wagner, G. A. *Primary and interlaboratory calibration of beta sources using quartz as thermoluminescent phosphor*. Ancient TL, (6): 2–6, 1979.

Porraz, G., Val, A., Tribolo, C., Mercier, N., de la Peña, P., Haaland, M. M., Igreja, M., Miller, C. E., and Schmid, V. C. *The MIS5 Pietersburg at '28' Bushman Rock Shelter, Limpopo Province, South Africa*. PLOS ONE, 13(10): e0202853–45, 2018. doi: 10.1371/journal.pone.0202853.

R Core Team. *R: A Language and Environment for Statistical Computing*. Vienna, Austria, 2018. URL https://r-project.org.

Soriano, S., Villa, P., Delagnes, A., Degano, I., Pollarolo, L., Lucejko, J. J., Henshilwood, C., and Wadley, L. *The Still Bay and Howiesons Poort at Sibudu and Blombos: Understanding Middle Stone Age Technologies*. PLOS ONE, 10(7): e0131127–46, 2015. doi: 10.1371/journal.pone.0131127.

Thomsen, K. J., Murray, A. S., Buylaert, J. P., Jain, M., Hansen, J. H., and Aubry, T. *Testing single-grain quartz OSL methods using sediment samples with independent age control from the Bordes-Fitte rockshelter (Roches d'Abilly site, Central France)*. Quaternary Geochronology, 31(C): 77–96, 2016. doi: 10.1016/j.quageo.2015.11.002.

Tindahl Madsen, A., Murray, A. S., and Joest Andersen, T. *Optical Dating of Dune Ridges on Rømø, a Barrier Island in the Wadden Sea, Denmark*. Journal of Coastal Research, 23(5): 1259–12, 2007. doi: 10.2112/05-0471.1.

Tolksdorf, J. F., Klasen, N., and Hilgers, A. *The existence of open areas during the Mesolithic: evidence from aeolian sediments in the Elbe–Jeetzel area, northern Germany*. Journal of Archaeological Science, 40(6): 2813–2823, 2013. doi: 10.1016/j.jas.2013.02.023.

Tribolo, C., Mercier, N., Douville, E., Joron, J. L., Reyss, J. L., Rufer, D., Cantin, N., Lefrais, Y., Miller, C. E., Porraz, G., Parkington, J., Rigaud, J. P., and Texier, P. J. *OSL and TL dating of the Middle Stone Age sequence at Diepkloof Rock Shelter (South Africa): a clarification*. Journal of Archaeological Science, 40 (9): 3401–3411, 2013. doi: 10.1016/j.jas.2012.12.001.

Turner, F., Tolksdorf, J. F., Viehberg, F., Schwalb, A., Kaiser, K., Bittmann, F., von Bramann, U., Pott, R., Staesche, U., Breest, K., and Veil, S. *Lateglacial/early Holocene fluvial reactions of the Jeetzel river (Elbe valley, northern Germany) to abrupt climatic and environmental changes*. Quaternary Science Reviews, 60: 91–109, 2013. doi: 10.1016/j.quascirev.2012.10.037.

Valladas, G. *A gamma ray irradiator*. PACT 3 - Revue du Réseau Européen de Sciences et Techniques appliquées au Patrimoine Culturel, pp. 439–442, 1978.

X-5 Monte Carlo Team. *MCNP — A General Monte Carlo N-Particle Transport Code, Version 5*. 2003. URL https://laws.lanl.gov/vhosts/mcnp.lanl.gov/mcnp5.shtml.

Reviewer

David Sanderson

Ancient TL

Athermal stability, bleaching behavior and dose response of luminescence signals from almandine and kyanite

Ian del Río[1*], André Oliveira Sawakuchi[2], Daniele Giordano[3], Thays Desiree Mineli[2], Luciana Nogueira[2], Tsegaye Abede[4], Daniel Atencio[2]

[1] Departamento de Ciencias Geológicas, Universidad Católica del Norte, Avenida Angamos 0610, Antofagasta, Chile
[2] Department of Sedimentary and Environmental Geology, Institute of Geosciences, University of São Paulo, Rua do Lago 562, São Paulo, SP, 05508-080, Brazil
[3] Earth Sciences Department, University of Torino, Via Valperga Caluso 35, 10125, Torino, Italy
[4] Adana Geological Consulting Company, Via Martin Luther King 9, 56021, Cascina, Italy

*Corresponding Author: iandelriogarcia@gmail.com

Received: April 4, 2019; in final form: June 18, 2019

Abstract

In order to evaluate the suitability of minerals other than quartz and feldspar for luminescence dating of sediments, luminescence properties from almandine and kyanite relevant for dosimetry such as luminescence signal stability, bleachability by sunlight exposure, and dose response are investigated. Thermoluminescence (TL) signals (UV emission) from almandine aliquots present athermal instability for the entire tested TL temperature range (25 – 450 °C). Almandine also presents a significant infrared stimulated luminescence (IRSL), post-infrared IRSL (post-IR IRSL) and optically stimulated luminescence (OSL) (blue stimulation and UV detection) signals. Kyanite aliquots show a TL glow curve (UV emission) characterized by four distinct peaks at temperatures of around 90, 170, 220 and 325 °C. The 325 °C TL peak seems to be stable, without significant decay after 6.8 hours of storage at room temperature (25 °C). Kyanite aliquots did not yield significant IRSL or post-IR IRSL signals, but OSL is observed in the UV detection window. Fading tests for the OSL signals resulted in g-values of 15.8 ± 2.8 %/decade for almandine and 21.2 ± 11.6 %/decade for kyanite. The OSL signals are bleachable by sunlight with 34% to 50% of signal remaining after 5 minutes of light exposure. Both minerals yielded dose recovery ratios close to unity (given dose of 100 Gy) and the dose response curves had a high D_0 values of around 800 Gy.

Keywords: Thermoluminescence; IRSL; OSL; Almandine; Kyanite; Luminescence dating

1. Introduction

Although quartz and feldspar are the major components of terrigenous sediments, the heavy mineral suite (density >2.85 g/cm^3) includes several minerals whose luminescence properties have been poorly investigated for dating purposes. In this context, silicates from the garnet group such as almandine ($Fe_3Al_2(SiO_4)_3$, ~ 4.31 g/cm^3) and aluminosilicates such as kyanite ($Al_2(SiO_4)O$, ~ 3.67 g/cm^3) are typical minerals in the heavy mineral assemblage of sands worldwide (Morton & Hallsworth, 1994, 1999). Both minerals occur in metamorphic rocks that experienced medium to high pressure and temperature conditions (100 – 2000 MPa and 200 – 1000 °C) equivalent to greenschist and eclogite facies (Deer et al., 2013). These rocks are common sources of sediments in cratonic geological settings like Brazil (Almeida et al., 2000). Almandine and kyanite show high resistance to physical and chemical weathering in comparison to other com-

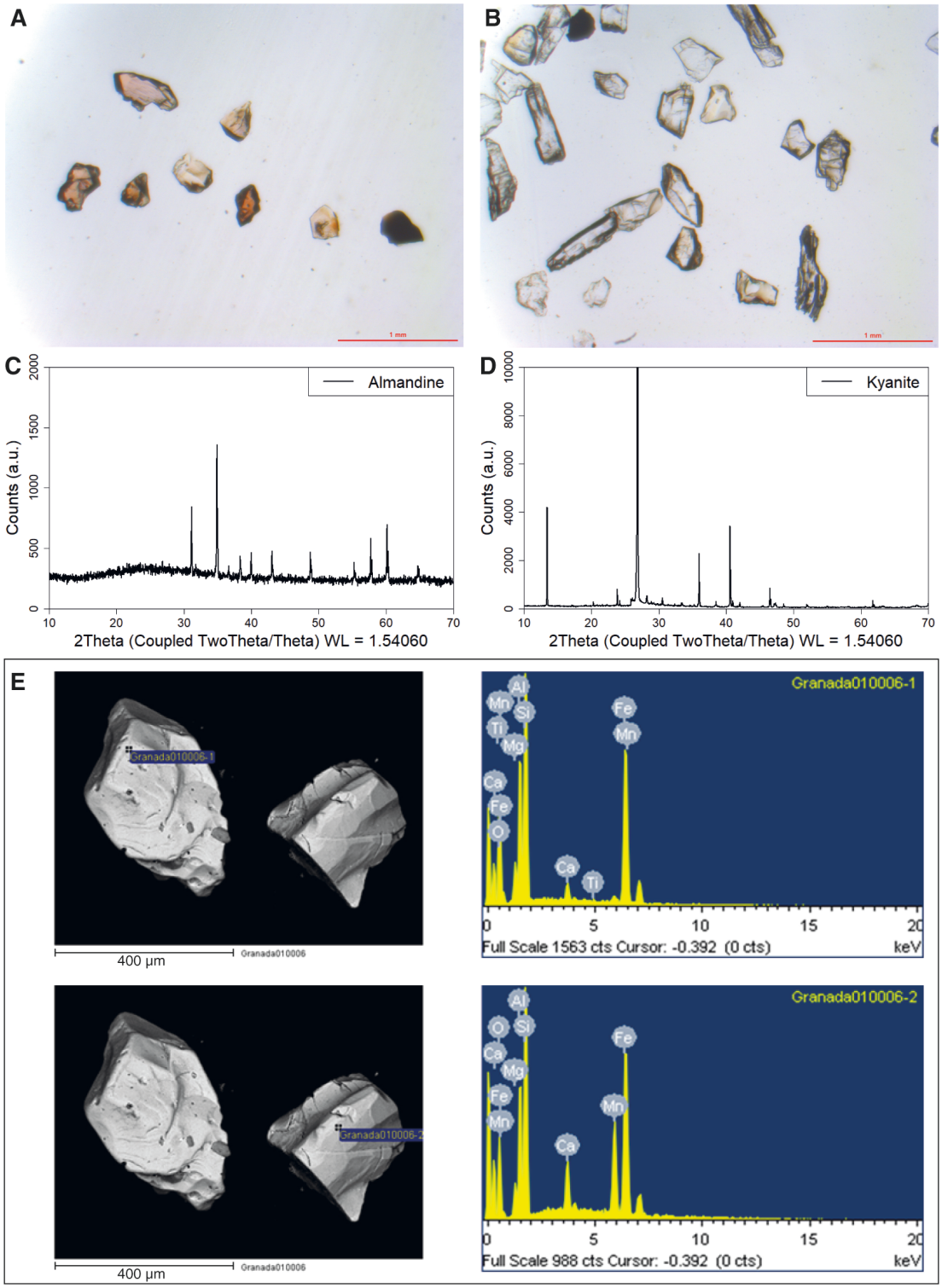

Figure 1. Almadine (A) and kyanite (B) grains under the optical microscope. XRD spectra of studied almandine (C) and kyanite (D) samples. E) Scanning electron microscope image (secondary electrons detector, left) from grains of almandine and energy dispersive spectrum (right) showing the chemical composition corresponding to the points highlighted in the images at left.

mon heavy minerals such as pyroxene and amphibole (Morton & Hallsworth, 1999). This property allows their transport over long distances and preservation in sediments. Detrital grains of almandine and kyanite typically account for between 5 and 20% of the heavy mineral suite of sands (Morton & Hallsworth, 1999; Rimington et al., 2000; Guedes et al., 2011; do Nascimento Jr et al., 2015).

Among the few studies on luminescence signals of heavy

Step	Procedure
1	Dose D_x
2	Preheat at 200°C for 10s
3	Blue stimulation at 125°C for 40s (L_x)
4	Test dose Dt
5	Preheat at 160°C for 0s
6	Blue stimulation at 125°C for 40s (T_x)
7	Blue stimulation at 280°C for 40s
8	Return to 1

Table 1. Measurement protocol (Murray & Wintle, 2003) applied to build dose response curves and estimate equivalent doses using the OSL signal from almandine and kyanite.

minerals, Watanabe et al. (2015) demonstrated that heavy minerals such as beryl and pyroxene show thermoluminescence (TL) signals with dose response curves reaching high saturation doses (>1000 Gy) compared to quartz optically stimulated luminescence (OSL) and feldspar infrared stimulated luminescence (IRSL) or post-infrared IRSL (post-IR IRSL) signals. However, the TL signals measured by Watanabe et al. (2015) as well as other previous studies that focused on TL signals of heavy minerals such as synthetic diopside-like crystals (Cano et al., 2008), kyanite (Souza et al., 2003) and andalusite (Cano et al., 2011) did not evaluate the dose response curves of luminescence signals corrected for sensitivity changes, and no information was provided for OSL or post-IR IRSL signals successfully used for luminescence dating.

This contribution investigates TL, OSL, IRSL and post-IR IRSL signals from almandine and kyanite. Particularly for the OSL signal, this includes the evaluation of bleaching performance, fading rates and dose response curves from both minerals.

2. Materials and methods

The studied almandine and kyanite crystals were obtained from the mineral collection of the Istituto di Geoscienze e Georisorse (Pisa, Italy). All samples were mechanically crushed and wet sieved to isolate the 180 – 250 µm grain-size interval. The purity of almandine and kyanite concentrates were assessed by means of optical microscopy (Fig. 1A, 1B) and X-ray diffraction (XRD) analysis (Fig. 1C, 1D). Scanning electron microscopy with energy dispersive spectroscopy (SEM/EDS) showed that the studied almandine grains contain relatively low amounts of magnesium. Since iron was the most abundant cation found in the studied samples (Fig. 1E), in the following section, we will refer to the mineral species as almandine for clarity.

Luminescence measurements were performed using a Risø TL/OSL DA-20 reader equipped with a $^{90}Sr/^{90}Y$ beta source, delivering a dose rate of 0.111 ± 0.003 Gy/s for discs and 0.099 ± 0.003 Gy/s for cups. We highlight that these beta source dose rates were determined using a quartz (2.65 g/cm^3) calibration standard (Hansen et al., 2015) which has lower density than almandine (~ 4.31 g/cm^3) and kyanite (~ 3.67 g/cm^3). Nathan et al. (2003) found a difference of ~ 30% for the beta dose rates in steel (7.9 g/cm^3) and glass (2.65 g/cm^3) spheres. Thus, the doses given in this study for almandine and kyanite aliquots are apparent doses. The mentioned doses are not accurate and must be considered only for evaluation of luminescence properties.

Optical stimulation used arrays of blue LEDs (470 ± 20 nm) at 90% power density (~ 40 mW/cm^2) and IR LEDs (870 ± 20 nm) also at 90% power density (~ 130 mW/cm^2). Light emissions were recorded through a Thorn EMI 9235QB photomultiplier. The OSL signal was measured with blue stimulation and light detection in the UV spectral range (290-370 nm) using a Hoya U-340 detection filter. The IRSL and post-IR IRSL signals were measured in the blue-violet window (340-480 nm) using a Corning 7-59 and Schott BG-39 filter combination. The TL emission was recorded both in the UV and blue-violet windows. Grains of almandine or kyanite were mounted on stainless steel discs (9.7 mm diameter) and cups (11.7 mm diameter) using silicone spray. Each aliquot contained ~ 500 grains covering the entire disc or cup to maximize signal intensity. Also, large aliquots minimize potential effects induced by variation in composition (i.e. cation concentration) of almandine grains from different aliquots.

After irradiating the almandine and kyanite aliquots with doses of 50, 100, 500 and 1000 Gy, TL glow curves were obtained in the UV and blue-violet detection windows. TL measurements were performed from room temperature (~ 25 °C) to 450 °C using a heating rate of 5 °C/s. In order to assess the stability of TL peaks and detect athermal loss of signal, or fading, aliquots from almandine and kyanite were irradiated with 200 Gy and TL signals were measured after storage at room temperature (~ 25 °C) for increasing times (0 to 6.82 hours) following an approach, similar to the fading measurements for IRSL signals (Auclair et al., 2003). Additionally, the response of TL signals to light exposure was evaluated for both minerals. For this experiment, a 200 Gy dose was administered to two aliquots of each mineral, which were exposed to a solar simulator lamp for 0, 2.5 and 5 hours.

The presence of IRSL (at 50 °C) and post-IR IRSL signals was checked for aliquots of almandine and kyanite. Aliquots were irradiated with 50 Gy and preheated at 250 °C (60 s) or 320 °C (60 s) for measurement of post-IR IRSL signals at 225 °C for 100 s (Buylaert et al., 2009) or at 290 °C for 200 s (Buylaert et al., 2012), respectively.

The OSL decay curves (100 s of blue light stimulation at 125 °C) were recorded for aliquots irradiated with 100 Gy and preheated for 10 s at temperatures of 25, 160, 200, 220, 260 and 300 °C. Linear modulated optically stimulated luminescence (LM-OSL) curves were obtained by linearly increasing the blue LED power intensity from 0 to 90% for 5000 s after giving a 200 Gy dose and a 200 °C preheat (10 s). The preheat temperature applied in LM-OSL measurements was defined after evaluation of the OSL signal depletion for preheat temperatures from 25 to 300 °C. A preheat temperature of 200 °C was used based on the intensity of initial

emission of the OSL decay curve of both minerals. This preheat temperature apparently eliminates less stable components, but still preserves a detectable emission in the initial 1 s of the OSL decay curve, which is analogous to the fast OSL component of quartz (Jain et al., 2003). The OSL signal measured with a preheat treatment at 200 °C for 10 s and corrected for a test dose signal (Table 1) was used in experiments to evaluate fading rate, bleachability and dose response.

The OSL signal was calculated from the first second of the OSL decay curve and the last 10 seconds were used as background. Fading rates for the OSL signal were estimated following Auclair et al. (2003). For this, three aliquots of each mineral type were irradiated with a 300 Gy dose, preheated to 200 °C and stimulated with blue LEDs after storage times between 0.4 and 55 hours. Sensitivity variation between measurements was corrected by a test dose of 100 Gy. In this study, g-values were calculated following Huntley & Lamothe (2001) and normalized to a measurement delay time of 2 days after irradiation.

The bleachability of the OSL signal was examined by administering a dose of 50 Gy to aliquots exposed to a solar simulator lamp from 5 minutes to 5 hours. Before each measurement, the aliquots were preheated to 200 °C. The dose response of the OSL signal was evaluated using a single-aliquot regenerative (SAR) dose protocol (Murray & Wintle, 2003) as described in Table 1. The dose response curves were built by administrating increasing doses (D_1<D_2<D_3<D_4) up to 2500 Gy and a test dose (D_t) of 100 Gy to control sensitivity changes during consecutive measurements. A 0 Gy dose (D_5) was given to estimate recuperation and a repetition of the first cycle (D_6 = D_1) to calculate the recycling ratio. A single saturating exponential growth function was used for fitting the dose response curves and calculation of characteristic dose (D_0). To assess the ability of OSL from the studied almandine and kyanite aliquots to recover a known dose under laboratory conditions, a dose recovery test was performed for a given dose of 100 Gy and using the protocol described in Table 1. Grain samples were exposed to light for long time (> 1 year) during their storage as museum specimens. The aliquots were further stimulated with blue light for 200 s at 280 °C prior to dose recovery tests, ensuring the

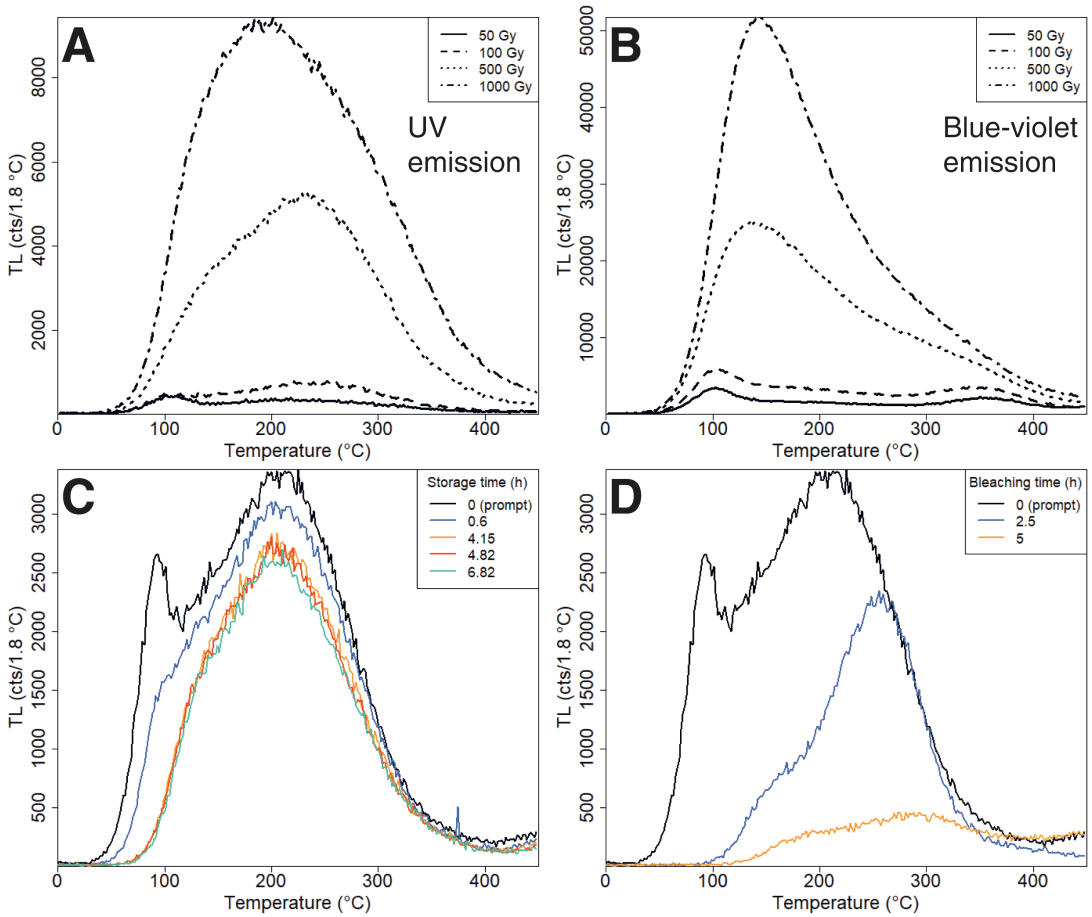

Figure 2. TL glow curves for the UV (A) and blue-violet (B) emissions of almandine. C) TL glow curves recorded after different storage times at room temperature (given dose of 200 Gy). D) TL glow curves recorded after different bleaching times under a solar simulator lamp. Note that the same TL measurement (0 storage or bleaching time) is used as reference for both stability and bleaching tests. Successive measurements were performed on the same aliquots.

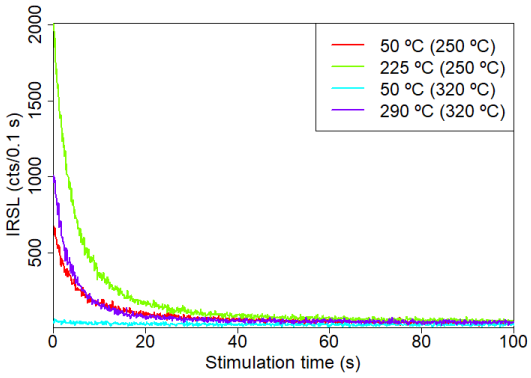

Figure 3. IRSL (at 50°C) and post-IR IRSL (at 225 and 290 °C) signals from almandine. For the IRSL and post-IR IRSL signals measured after a preheat of 320 °C, only the first 100 s of light emission are shown. The preheat temperatures are shown in brackets.

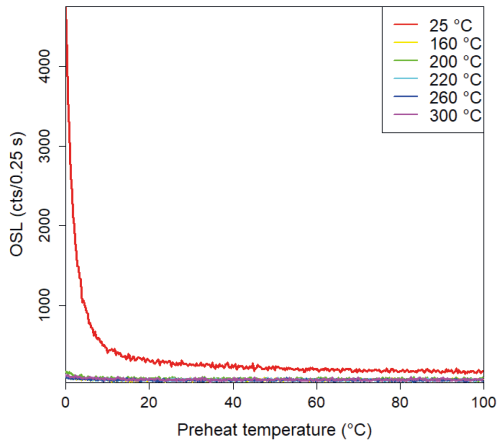

Figure 4. OSL decay curves of almandine measured for different preheat temperatures (from 25 to 300 °C). Aliquots were irradiated with 100 Gy.

bleaching of signals from natural residual doses. The data analysis were performed using the software *Analyst* (v4.52; Duller 2015) and the **R** package `'Luminescence'` (Kreutzer et al., 2012).

3. Results

3.1. Almandine

For the UV detection window, almandine TL curves (Fig. 2A) exhibit a peak at 100 °C, more noticeable at lower doses (50 Gy), followed by a broad peak from 150 to 350 °C, centered at about 220 °C. For doses higher than 100 Gy, a broad TL peak appears centered in the 200 – 240 °C interval, merging with the 100 °C peak and hindering the identification of other peaks. In the blue-violet detection window, TL peaks at 100 and 360 °C are recognized at doses up to 100 Gy. At higher doses, the 360 °C peak is hidden below the broad tail of the 100 °C peak (Fig. 2B). The TL (UV emission) of almandine aliquots decays significantly after 0.5 hours of storage under room temperature, but this is more notable for the 100°C TL peak (Fig. 2C). Regarding the bleachability of TL in the UV emission, the 100 °C TL peak was totally depleted after 2.5 hours of light exposure (Fig. 2D). However, the high instability of this peak at room temperature hinders the evaluation of its bleaching rate. After 5 hours of light exposure, there is significant depletion of the TL curve (25 – 450 °C) with a low intensity peak at 300 °C. Higher temperature TL peaks (> 200 °C) are highly depleted when aliquots are exposed to light, pointing to a significant bleaching (Fig. 2D).

Almandine shows significant IRSL and post-IR IRSL signals (Fig. 3). IRSL signals measured at 50 °C have a lower intensity than post-IR IRSL signals measured at 225 or 290 °C.

The OSL intensity from almandine decreases with the increase of preheat temperature (Fig. 4). OSL decay curves measured after a preheat with temperature from 160 to 300 °C display intensities (initial 1 s) almost 40 times lower than OSL curve obtained without preheat ("room temperature preheat" of 25 °C) (Fig. 4). The LM-OSL curve shows a well-defined peak in the first 100 s of light stimulation (Fig. 5A). Deconvolution into discrete components suggests the presence of four OSL components with photoionisation cross-section values of $1.21 \pm 0.13 \times 10^{-17}$, $1.68 \pm 0.18 \times 10^{-18}$, $8.87 \pm 2.8 \times 10^{-20}$ and $6.23 \pm 1.1 \times 10^{-22}$ cm^2.

Fading tests confirm the presence of athermal loss of the studied OSL signal from almandine that can be well-described as a logarithmic decay. The estimated average g-value is 15.8 ± 2.8 %/decade (Fig. 5B). The OSL signal decreases with light exposure (Fig. 5C). After 5 minutes of light exposure, remaining OSL signals amount to 34% of the initial signal (50 Gy). After 5 hours of light exposure, the OSL signal remaining is 8% of the initial signal. The dose response curve (Fig. 5D) of the OSL signal is well described by a single-saturating exponential function, showing relatively high saturation levels, with an average D_0 value of 791 Gy (n=2). Dose recovery tests resulted in an average calculated-to-given ratio of 0.98 ± 0.04 (for a given dose of 100 Gy), with aliquots yielding recuperation less than 0.1% and an average recycling ratio of 1.07 ± 0.04 (Table 2).

3.2. Kyanite

In the UV emission, kyanite TL curves reveal peaks at 90, 170, 220 and 325 °C (Fig. 6A). The TL peaks at 170, 220 and 325 °C grow up to a dose of 1000 Gy while the 90 °C TL peak reaches saturation at lower doses. TL curves of the blue-violet emission resemble the TL in the UV emission, with peaks at 90, 170 and 220 and a lower intensity peak at 325 °C (Fig. 6B). TL peaks (UV emission) of kyanite show differential decay when aliquots are stored under room temperature, with peaks at 90 and 170 °C presenting faster decay (Fig. 6C). However, the 325 °C TL peak is relatively stable for storage times up to 6.82 hours. Intensities of the 90, 170

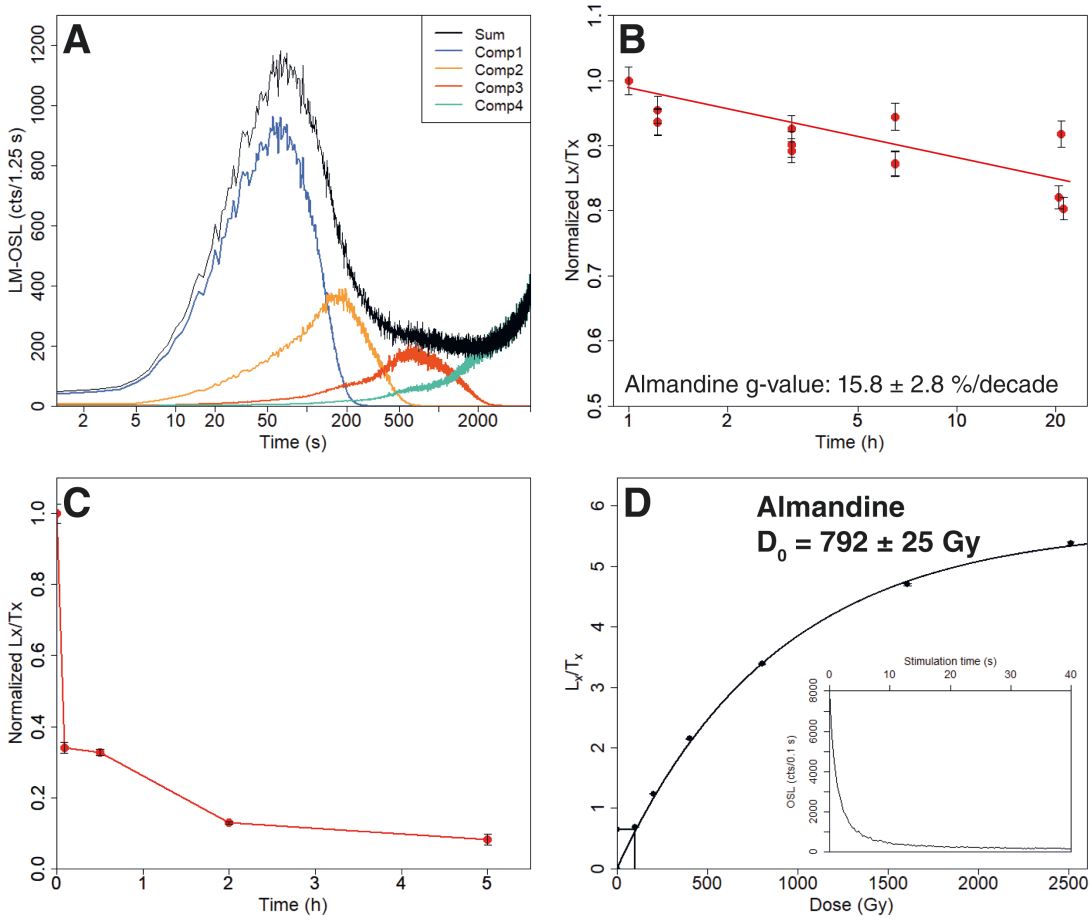

Figure 5. A) LM-OSL curve of almandine aliquot after a given dose of 200 Gy. Four OSL components resulted from deconvolution of the LM-OSL curve. B) Athermal decay of the OSL signal, with calculated g-value. C) Bleaching behavior represented by decay of the OSL signal in terms of light exposure time. D) Dose response curve showing the characteristic dose value (D_0)

and 325 °C TL peaks were determined from integration intervals of ± 20 °C centered at the corresponding TL peak (Fig. 7). A lower decrease rate is observed for the TL peak at 170 °C compared to the 90 °C TL peak (Fig. 7). As suggested by observation of the TL glow curves, the 325 °C TL peak shows stability under room temperature for the studied time interval (Fig. 7). All observed TL peaks decays with exposure to the solar simulator lamp (Fig. 6D).

IRSL and post-IR IRSL emission (blue-violet detection window) from kyanite aliquots show negligible intensities, impeding detection of signal over the observed background. The OSL decay curves of kyanite aliquots have decreasing intensities for higher preheat temperatures (Fig. 8). The LM-OSL emission has relatively low intensity, with a low peak at around 200 s. The low luminescence sensitivity of the kyanite impeded the identification of individual OSL components from the LM-OSL curves (Fig. 9A). Fading tests resulted in variable g-values from 10.4 to 33.6 %/decade with an average of 21.2 ± 11.6 %/decade (Fig. 9B). When exposed to a solar simulator lamp, the OSL signal (50 Gy) progressively decreases, confirming its bleachability (Fig. 9C). After 5 minutes of light exposure, the remaining OSL signal is around 50% of the initial signal. The remaining signal is 4% of the initial OSL signal after 5 hours of light exposure. The dose response curve is well described by a single-saturating exponential function (Fig. 9D), pointing to

Mineral	Calculated dose (Gy)	Calculated-to-given dose ratio	Recuperation (%)	Recycling ratio	D_0 (Gy)
Almandine	98.8 ± 4.4	0.98 ± 0.04	<0.1%	1.07 ± 0.04	791 ± 1
Kyanite	99.2 ± 9.3	0.99 ± 0.09	<0.1%	1.21 ± 0.16	1080 ± 139

Table 2. Summary of dose recovery test for a 100 Gy given dose. The results are the average of two aliquots. Measurement protocol described in Table 1.

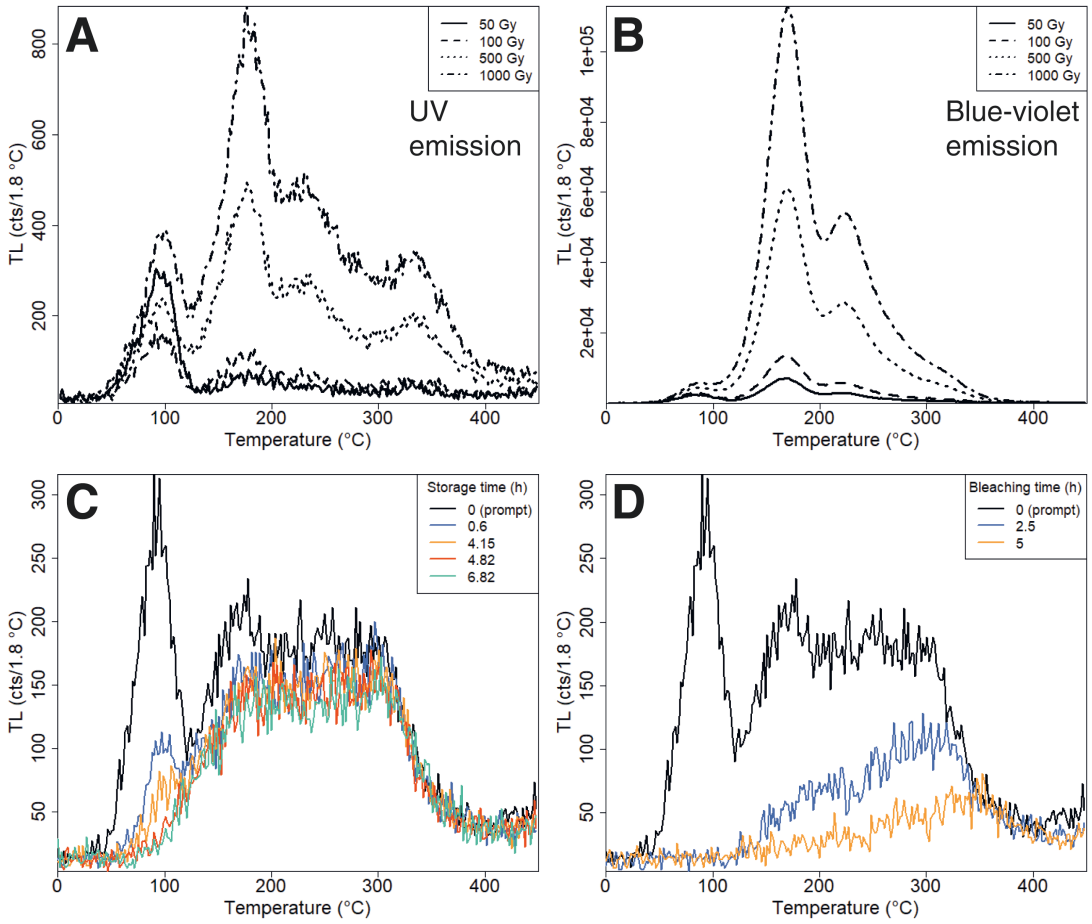

Figure 6. TL glow curves for the UV (A) and blue-violet (B) emissions from kyanite aliquots. C) TL glow curves obtained after different storage times at room temperature (given dose of 200 Gy). D) TL glow curves recorded after different bleaching times under a solar simulator lamp. Note that the same TL glow curve is used as reference for both stability and bleaching tests. Successive measurements were performed on the same aliquots.

an average D_0 value of 1080 Gy (n=2). Dose recovery tests present calculated-to-given dose ratio of 0.99 ± 0.09, with aliquots showing negligible recuperation (< 0.1%) and average recycling ratio of 1.21 ± 0.16 (Table 2).

4. Discussion

Almandine and kyanite are common detrital minerals in sandy sediments (Morton & Hallsworth, 1994, 1999) and they can potentially record equivalent doses used to determine sediment burial ages. Furthermore, these minerals are common in metamorphic rocks and their TL and OSL properties can be explored for surface exposure dating (Sohbati et al., 2012) and for low temperature thermochronology (King et al., 2016). Previous difficulties in isolating specific heavy minerals for luminescence dating (van Es et al., 2002) could be surpassed combining spatially resolved luminescence measurements (Kook et al., 2015) and mineral chemistry analysis using micro X-ray fluorescence methods (Thomsen et al., 2018). In this study, almandine shows a broad TL peak and IRSL and post-IR IRSL emissions, which are analogous to the luminescence characteristics of feldspar (Bøtter-Jensen et al., 1994; Blair et al., 2005). Kyanite has several discrete TL peaks, located approximately at 90, 170, 220 and 325 °C, as well as absence of IRSL emission, resembling the luminescence characteristics of quartz (Krbetschek et al., 1997). TL signals from almandine aliquots show instability as their TL intensities decreases with storage time at room temperature. Kyanite also presents unstable TL peaks, with exception of the TL peak at 325 °C. Both minerals present TL peaks sensitive to light. The TL glow curve from kyanite (Fig. 6) presents a behavior similar to quartz TL as it also displays a so-called "Rapidly Bleaching Peak" (RBP) at lower temperature (90 °C) and a "Slowly Bleaching Peak" (SBP) at higher temperature (325 °C) (Martini et al., 2009). The TL peak at 325 °C of kyanite decreases to around 30 – 40% of its initial intensity after 5 hours of light exposure, which is a rate similar to IRSL and post-IR IRSL signals from potassium feldspar (Buylaert et al., 2012). However, our experiments are unsuitable to discriminate the decay of

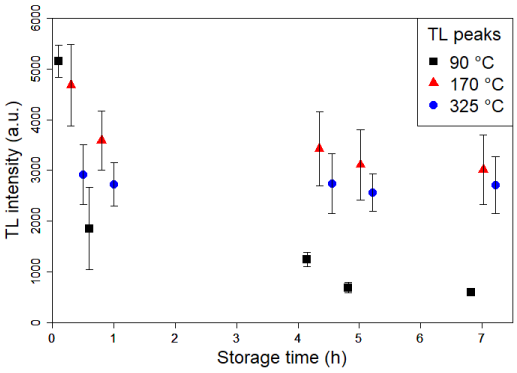

Figure 7. Intensity variation of TL peaks at 90, 170 and 325 °C (given dose of 200 Gy) from kyanite aliquots irradiated with 200 Gy and stored at room temperature for different times (storage time). Each TL intensity point is represented by the average of two aliquots. Data points are offset in the x axis to avoid points overlapping.

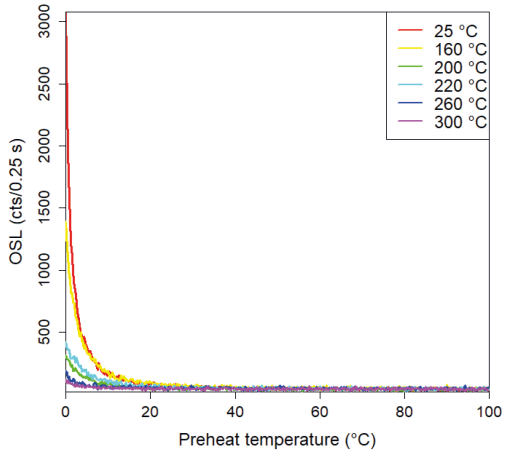

Figure 8. OSL decay curves of kyanite measured for different preheat temperatures (from 25 to 300 °C). Aliquots were irradiated with 100 Gy.

TL peaks from almandine and kyanite in terms of thermal or light bleaching effects. For example, such a loss of TL signal during storage at room temperature and light exposure experiments could be the result of thermal quenching, causing a reduced efficiency of the luminescence response to a given dose when the increase of temperature led to electrons recombining through non-radiative centers (Pagonis et al., 2010). Nonetheless, the difference in signal behavior between the TL curves obtained for the storage time (Fig. 2C, 6C) and bleaching experiments (Fig. 2D, 6D) cannot be explained entirely by thermal quenching since the main measurement parameters (i.e. heating rate, maximum temperature, given dose and dose rate) were the same during both experiments. Further experiments should be performed to clarify the process responsible for decay of TL signals observed in almandine and kyanite.

Both almandine and kyanite show an OSL emission in the UV band (blue stimulation). The OSL decay curve of almandine can comprise four OSL components. The OSL sensitivity of kyanite is extremely low (~ 0.5 cts Gy^{-1} mg^{-1} for the first second of light emission) which could hamper measuring doses below 100 Gy. The OSL signals from almandine and kyanite have relatively high fading rates, respectively with average g-values of 15.8 ± 2.8 %/decade and 21.2 ± 11.6 %/decade (Fig. 5B,9B), which are higher than g-values reported for the OSL signal from feldspar measured with blue stimulation and UV detection (g-value = 3.2 ± 0.2 %/decade, (Thomsen et al., 2008). The high variation in g-values found for kyanite points that fading rate should be estimated for individual aliquots for equivalent dose correction purposes. Also, due to such high g-values, signal loss during irradiation must be included in the estimation.

The OSL signals from almandine and kyanite decay to 10% of their initial value after 5 hours of exposure to a solar simulator lamp (Fig. 5C, 9C). This bleaching rate is also similar to that presented by feldspar IRSL and post-IR IRSL signals (Buylaert et al., 2012). In this case, residual signals for both minerals can promote significant dose overestimation and should be evaluated, especially for sediments experiencing fast deposition and short light exposure periods like in alluvial fans or braided rivers. The studied almandine and kyanite have dose response curves with D_0 reaching values higher than 700 Gy (Fig. 5D, 9D), which is beyond quartz OSL (Murray & Wintle, 2003) and similar to potassium feldspar post-IR IRSL (Buylaert et al., 2012). Dose recovery tests demonstrate the suitability of the studied minerals to recover a given dose (100 Gy) under laboratory conditions. However, the high fading rates are challenging for estimation of natural doses and potential extension of the age limit of luminescence dating.

Regarding dose rate assessment, uranium (^{238}U and ^{235}U), thorium (^{232}Th) and potassium (^{40}K) can occur as impurities in almandine and kyanite, contributing to significant internal dose rate. Almandine forms part of the garnet group that can be defined by the general formula $X_3Y_2(SiO_4)_3$, where the X position can be occupied by divalent cations of Ca^{2+}, Mg^{2+}, Fe^{2+} and Mn^{2+} and the Y position corresponds to trivalent cations as Al^{3+}, Fe^{3+} and Cr^{3+} (Deer et al., 2013). Almandine represents the ferric extreme ($Fe^{2+}{}_3Al_2(SiO_4)_3$) of the iron-magnesium solid solution series while pyrope is the magnesium extreme ($Mg_3Al_2(SiO_4)_3$). Kyanite is an aluminosilicate with general formula $Al_2(SiO_4)O$ and has andalusite and sillimanite as polymorphs (Deer et al., 2013). In the particular case of K, which promotes significant internal dose rate in potassium feldspar (Huntley & Baril, 1997), its relatively large atomic radius (Shannon, 1976) prevents substitution into the crystal lattice of both almandine and kyanite. However, chemical analysis on garnet crystals within metamorphic rocks (skarn) from Scotland (United Kingdom) indicates that the content of uranium could exceed 300 ppm (Smith et al., 2004) and in that case alpha particles are important contributors of the dose rate and most dose could be internal. This opens the possibility to explore chronometers

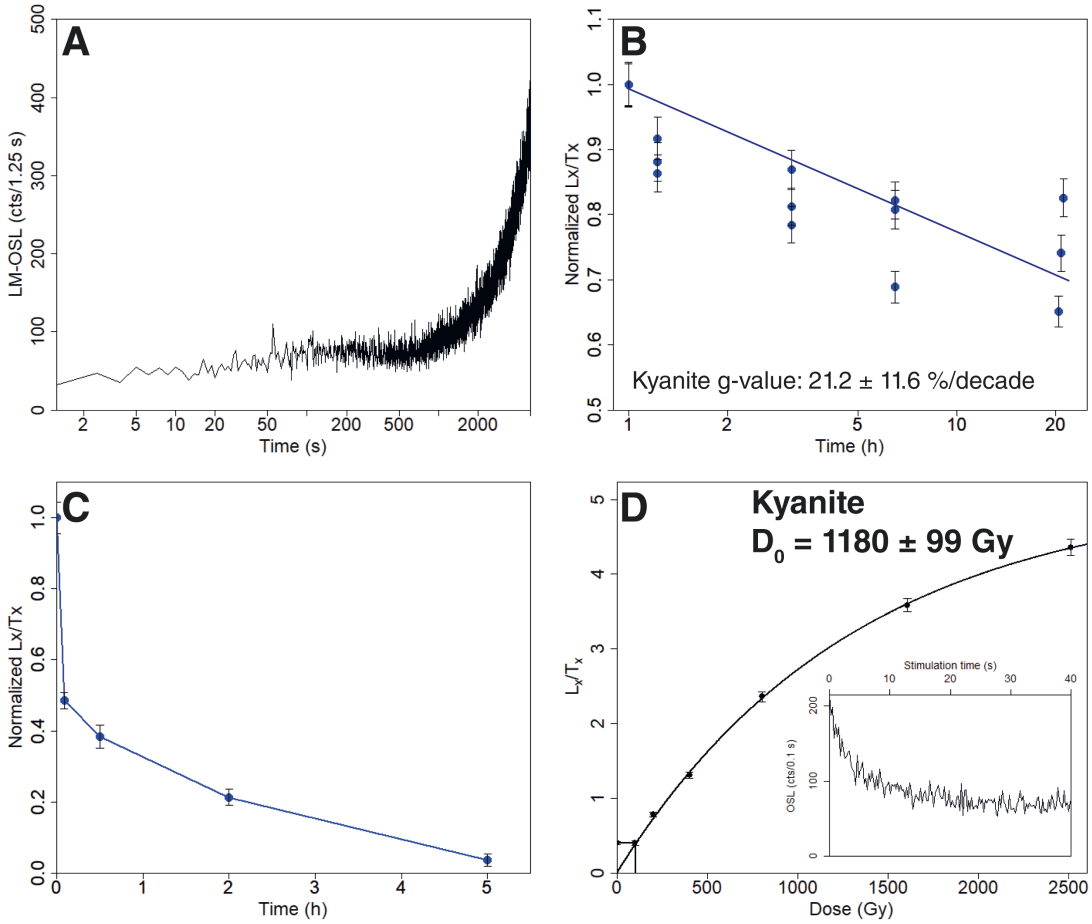

Figure 9. A) LM-OSL curve from a kyanite aliquot irradiated with 200 Gy. B) Athermal decay of the OSL signal, with calculated g-value. C) Bleaching behavior represented by decay of the OSL signal in terms of light exposure time. D) Dose response curve and calculated D_0 value.

based on natural regenerated signals like the method proposed for zircon (Smith, 1988; van Es et al., 2002). In such case, the assessment of radionuclides concentrations in minerals of the garnet group, like almandine, is needed for calculation of internal dose rate. In the studied almandine crystals, however, significant concentrations of U, Th or K were not detected using SEM/EDS (Fig. 1E).

5. Conclusions

IRSL and post-IR IRSL signals were observed only in almandine. Particularly, optical bleaching and stability of the 325 °C TL peak from kyanite deserve future investigations to evaluate its use for equivalent dose estimation. The OSL signals of almandine and kyanite are bleachable, with less than 10% of the initial signals remaining after 5 hours of light exposure. They present high saturation doses ($2D_0$ > 1500 Gy) that could extend the luminescence dating age limit beyond the mid Pleistocene, assuming dose rates of ~ 1 Gy/ka, typical of quartz-rich sands and of minerals hosting insignificant amounts of radionuclides. Dose recovery tests demonstrated that the studied heavy minerals can recover a given dose within unity under laboratory conditions. However, athermal stability and high fading rates of the studied OSL signal may entail a problem to obtain accurate equivalent doses estimates and ages. Future work should focus on searching for stable signals. Also, the investigation of the luminescence properties of other heavy minerals common in sediments (e.g. staurolite, sillimanite, titanite, apatite, epidote, rutile, tourmaline and zircon) is recommended for potential expansion of trapped-charged dating methods.

Acknowledgments

We are grateful to the Reviewer Prof. Ashok K. Singhvi for the insightful comments to improve the manuscript. We also thank the Editor Prof. Regina DeWitt for handling the manuscript. This research was conducted by funding provided by CONICYT (Chile) through the PhD Scholarship 21160616 provided to Ian Del Río. André O. Sawakuchi is supported by CNPq grant 304727/2017-2. We thank Dr. Flavio Machado de Souza Carvalho and Dr. Isaac Jamil Sayeg for their contributions with X-ray diffraction and SEM/EDS analysis.

References

Almeida, F. F. M., Brito Neves, B. B., and Carneiro, C. D. R. *The origin and evolution of the South American Platform* . Earth-Science Reviews, 50(1–2): 77–111, 2000. doi: 10.1016/S0012-8252(99)00072-0.

Auclair, M., Lamothe, M., and Huot, S. *Measurement of anomalous fading for feldspar IRSL using SAR*. Radiation Measurements, 37 (4–5): 487–492, 2003. doi: 10.1016/S1350-4487(03)00018-0.

Blair, M. W., Yukihara, E. G., and McKeever, S. W. S. *Experiences with single-aliquot OSL procedures using coarse-grain feldspars*. Radiation Measurements, 39(4): 361–374, 2005. doi: 10.1016/j.radmeas.2004.05.008.

Bøtter-Jensen, L., Duller, G. A. T., and Poolton, N. R. J. *Excitation and emission spectrometry of stimulated luminescence from quartz and feldspars*. Radiation Measurements, 23(2–3): 613–616, 1994. doi: 10.1016/1350-4487(94)90108-2.

Buylaert, J. P., Murray, A. S., Thomsen, K. J., and Jain, M. *Testing the potential of an elevated temperature IRSL signal from K-feldspar*. Radiation Measurements, 44(5–6): 560–565, 2009. doi: 10.1016/j.radmeas.2009.02.007.

Buylaert, J. P., Jain, M., Murray, A. S., Thomsen, K. J., Thiel, C., and Sohbati, R. *A robust feldspar luminescence dating method for Middle and Late Pleistocene sediments*. Boreas, 41: 435–451, 2012. doi: 10.1111/j.1502-3885.2012.00248.x.

Cano, N. F., Yauri, J. M., Watanabe, S., Mittani, J. C. R., and Blak, A. R. *Thermoluminescence of natural and synthetic diopside.* Journal of Luminescence, 128(7): 1185–1190, 2008. doi: 10.1016/j.jlumin.2007.11.090.

Cano, N. F., Blak, A. R., and Watanabe, S. *Electron paramagnetic resonance and the thermoluminescence emission mechanism of the 280 °C peak in natural andalusite crystal.* Journal of Luminescence, 131(7): 1545–1549, 2011. doi: 10.1016/j.jlumin.2011.02.014.

Deer, W. A., Howie, R. A., and Zussman, J. *An introduction to the rock-forming minerals*. Studies in archaeological science. Mineralogical Society of Great Britain and Ireland, 2013. doi: 10.1180/DHZ.

do Nascimento Jr, D., Sawakuchi, A., Guedes, C., Giannini, P., Grohmann, C., and Ferreira, M. *Provenance of sands from the confluence of the Amazon and Madeira rivers based on detrital heavy minerals and luminescence of quartz and feldspar*. Sedimentary Geology, 316: 1–12, 2015. doi: 10.1016/j.sedgeo.2014.11.002.

Duller, G. A. T. *The Analyst software package for luminescence data: overview and recent improvements* . Ancient TL, 33 (1): 35–42, 2015. URL http://ancienttl.org/ATL_33-1_2015/ATL_33-1_Duller_p35-42.pdf.

Guedes, C. C. F., Giannini, P. C. F., Nascimento Jr, D. R., Sawakuchi, A. O., Tanaka, A. P. B., and Rossi, M. G. *Controls of heavy minerals and grain size in a Holocene regressive barrier (Ilha Comprida, southeastern Brazil)*. Journal of South American Earth Sciences, 31(1): 110–123, 2011. doi: 10.1016/j.jsames.2010.07.007.

Hansen, V., Murray, A., Buylaert, J.-P., Yeo, E.-Y., and Thomsen, K. *A new irradiated quartz for beta source calibration*. Radiation Measurements, 81: 123–127, 2015. doi: 10.1016/j.radmeas.2015.02.017.

Huntley, D. J. and Baril, M. R. *The K content of the K-feldspars being measured in optical dating or in thermoluminescence dating*. Ancient TL, 15(1): 11–13, 1997. URL http://ancienttl.org/ATL_15-1_1997/ATL_15-1_Huntley_p11-13.pdf.

Huntley, D. J. and Lamothe, M. *Ubiquity of anomalous fading in K-feldspars, and the measurement and correction for it in optical dating*. Canadian Journal of Earth Sciences, 38(7): 1093–1106, 2001. doi: 10.1139/e01-013.

Jain, M., Murray, A., and Bøtter-Jensen, L. *Characterisation of blue-light stimulated luminescence components in different quartz samples: implications for dose measurement*. Radiation Measurements, 37(4-5): 441–449, 2003. doi: 10.1016/j.radmeas.2015.02.017.

King, G. E., Guralnik, B., Valla, P. G., and Herman, F. *Trapped-charge thermochronometry and thermometry: A status review*. Chemical Geology, 446(23): 3–17, 2016. doi: 10.1016/j.chemgeo.2016.08.023.

Kook, M., Lapp, T., Murray, A. S., Thomsen, K. J., and Jain, M. *A luminescence imaging system for the routine measurement of single-grain OSL dose distributions*. Radiation Measurements, 81(4-5): 171–177, 2015. doi: 10.1016/j.radmeas.2015.02.010.

Krbetschek, M. R., Götze, J., Dietrich, A., and Trautmann, T. *Spectral information from minerals relevant for luminescence dating*. Radiation Measurements, 27(506): 695–748, 1997. doi: 10.1016/S1350-4487(97)00223-0.

Kreutzer, S., Schmidt, C., Fuchs, M. C., Dietze, M., Fischer, M., and Fuchs, M. *Introducing an R package for luminescence dating analysis*. Ancient TL, 30(1): 1–8, 2012. URL http://ancienttl.org/ATL_30-1_2012/ATL_30-1_Kreutzer_p1-8.pdf.

Martini, M., Fasoli, M., and Galli, A. *Quartz OSL emission spectra and the role of [AlO4]° recombination centres*. Radiation Measurements, 44(5–6): 458–461, 2009. doi: 10.1016/j.radmeas.2009.04.001.

Morton, A. and Hallsworth, C. *Identifying provenance-specific features of detrital heavy mineral assemblages in sandstones*. Sedimentary Geology, 90(3–4): 241–265, 1994. doi: 10.1016/0037-0738(94)90041-8.

Morton, A. and Hallsworth, C. *Processes controlling the composition of heavy mineral assemblages in sandstones*. Sedimentary Geology, 124(1–4): 3–29, 1999. doi: 10.1016/S0037-0738(98)00118-3.

Murray, A. and Wintle, A. *The single aliquot regenerative dose protocol: potential for improvements in reliability*. Radiation Measurements, 37(4-5): 377–381, 2003. doi: 10.1016/S1350-4487(03)00053-2.

Nathan, R., Thomas, P., Jain, M., Murray, A., and Rhodes, E. *Environmental dose rate heterogeneity of beta radiation and its implications for luminescence dating: Monte Carlo modelling and experimental validation*. Radiation Measurements, 37(4-5): 305–313, 2003. doi: 10.1016/S1350-4487(03)00008-8.

Pagonis, V., Ankjaergaard, C., Murray, A., Jain, M., Chen, R., Lawless, J., and Greilich, S. *Modelling the thermal quenching mechanism in quartz based on time-resolved optically stimulated luminescence*. Journal of Luminescence, 130(5): 902–909, 2010. doi: 10.1016/j.jlumin.2009.12.032.

Rimington, N., Cramp, A., and Morton, A. *Amazon Fan sands: implications for provenance*. Marine and Petroleum Geolog, 17 (2): 267–284, 2000. doi: 10.1016/S0264-8172(98)00080-4.

Shannon, R. *Revised effective ionic radii and systematic studies of interatomic distances in halides and chalcogenides*. Acta Crystallographica, 32(5): 751–767, 1976. doi: 10.1107/S0567739476001551.

Smith, B. *Zircon from sediments: A combined OSL and TL autoregenerative dating technique*. Quaternary Science Reviews, 7 (3–4): 401–406, 1988. doi: 10.1016/0277-3791(88)90036-4.

Smith, M., Henderson, P., Jeffries, T., Long, J., and Williams, C. *The Rare Earth Elements and Uranium in Garnets from the Beinn an Dubhaich Aureole, Skye, Scotland, UK: Constraints on Processes in a Dynamic Hydrothermal System*. Journal of Petrology, 45(3): 457–484, 2004. doi: 10.1093/petrology/egg087.

Sohbati, R., Murray, A., Chapot, M., and Jain, M. *Optically stimulated luminescence (OSL) as a chronometer for surface exposure dating*. Journal of Geophysical Research, 117: B09202, 2012. doi: 10.1029/2012JB009383.

Souza, S., Selvin, P., and Watanabe, S. *Thermally stimulated luminescence, optical absorption and EPR studies on kyanite crystals*. Journal of Luminescence, 130(102-103): 575–580, 2003. doi: 10.1016/S0022-2313(02)00622-1.

Thomsen, K. J., Kook, M., Murray, A. S., and Jain, M. *Resolving luminescence in spatial and compositional domains.* Radiation Measurements, 120: 260–266, 2018. doi: 10.1016/j.radmeas.2008.06.002.

Thomsen, K., Murray, A., Jain, M., and Bøtter-Jensen, L. *Laboratory fading rates of various luminescence signals from feldspar-rich sediment extracts*. Radiation Measurements, 43(9–10): 1474–1486, 2008. doi: 10.1016/j.meas.2018.06.002.

van Es, H., Vainshtein, D., Rozendaal, A., Donoghue, J., Meijer, R., and den Hartog, H. *Thermoluminescence of ZrSiO4 (zircon): A new dating method?* Nuclear Instruments and Methods in Physics Research Section B: Beam Interactions with Materials and Atoms, 191(1-4): 649–652, 2002. doi: 10.1016/S0168-583X(02)00627-4.

Watanabe, S., Cano, N., Carmo, L., Barbosa, R., and Chubaci, J. *High- and very-high-dose dosimetry using silicate minerals*. Radiation Measurements, 72: 66–69, 2015. doi: 10.1016/j.radmeas.2014.11.004.

Reviewer

Ashok Singhvi

Thesis Abstracts

Index

Catherine Elizabeth Buckland

New methods for identifying dune system reactivation drivers and responses, Nebraska Sandhills

January 2019

School of Geography and the Environment, University of Oxford, South Parks Road, Oxford

Degree: Ph.D.

Supervisors: David Thomas, Richard Bailey

Two billion people living in drylands are affected by land degradation and the destabilisation of surface sediments. However, a detailed understanding of the combined effects of natural and anthropogenic factors in contributing to sediment remobilisation is absent from the literature. A quantified awareness of vegetation cover sensitivities and resultant land degradation to forcing factors is needed if the vegetation and landscape response to future climatic changes and human pressure are to be better predicted.

Measuring past environmental response in a location with a known disturbance history allows us to identify thresholds and explore the relationship between disturbance forces and sedimentary response within a dryland environment. The Nebraska Sandhills, located in the Central Great Plains, is a semi-arid dune field with a reactivation history spanning the last 10,000 years and a well-documented history of forcing factors over recent decades. Whilst regional reactivations in the Central Great Plains have largely been attributed to palaeoclimatic change, the role of humans (e.g. The Dust Bowl of the 1930s), in particular over grazing, has also been cited as a potential cause of land degradation and sediment reactivation.

Using quartz luminescence dating, secondary datasets of forcing factors and statistical inference methods, this thesis identifies the record of sediment deposition in near-surface aeolian stratigraphies in the northern remits of the Nebraska Sandhills and explores the relationship between environmental sensitivity and external disturbance factors. High-resolution luminescence techniques allow us to construct a detailed chronological history of sedimentary deposition events over the last 900 years, producing a record of the environmental response across a range of aeolian features within the semi-arid setting. Combined with a detailed history of climatic, grazing and wildfire pressures, supervised machine learning techniques explore the relationship between forcing factor and environmental response, highlighting the importance of both regional and localised conditions in contributing to the heterogeneous sedimentary response found in the record.

A PDF of this thesis can be downloaded from: https://ora.ox.ac.uk/objects/uuid:94b1a151-64fb-47af-a483-ab445979d413

Laura Eddey

The Late Quaternary Palaeoenvironment of the Vale of Pickering

December 2018

University of Sheffield, Sheffield, United Kingdom

Degree: Ph.D.

Supervisors: Mark Bateman, Stephen Livingstone, Jon Lee

During the Quaternary, repeated glacial cycles left widespread deposits across Britain. These deposits hold an archive of terrestrial responses to changes in climate over the last 2.6 Ma. One such archive is the Vale of Pickering in North Yorkshire: A low-lying depression bounded on all sides save the east end by large hills comprised of Jurassic and Cretaceous bedrock. During the Late Quaternary, this natural basin was blocked by ice sheets forming large proglacial lakes. To understand the advance and retreat of the surrounding ice lobes in the Vale of York to the west and the North Sea Lobe to the east – the deposits of the Vale of Pickering are crucial; however, limited work in the area has failed to ascertain an accurate history of Lake Pickering. Using newly available high-resolution LiDAR data, field observations, historic borehole records, and optically stimulated luminescence (OSL) dating, a new chronological model for Lake Pickering has been established. This shows that 1) previously estimated lake levels are too high and that during the LGM, Lake Pickering was no more than 33 m O.D. 2) Ice invaded the eastern coast of the Vale of Pickering on more than one occasion, potentially earlier than the LGM. 3) Several iterations of Lake Pickering exist with a lake during the LGM, but at least one older than 30 ka. 4) The drainage of Lake Pickering is very complex and seaward drainage likely prevailed until the eastern end became blocked by continued deposition of glacial material. This reversed the drainage through the Kirkham Gorge. 5) The use of newer geoscientific techniques like OSL and LiDAR mapping are crucial to the understanding of the palaeoenvironment of the Vale of

Pickering and the continued development of these techniques are vital to further work.

Geraint Jenkins

Development and application of luminescence dating of cobbles from glaciofluvial sediments

January 2019
Department for Geography and Earth Sciences, Aberystwyth University, Wales
Degree: Ph.D.
Supervisors: Department for Geography and Earth Sciences, Aberystwyth University, Wales

The aim of this thesis is to develop and test the luminescence dating of cobbles from glaciofluvial sediments. In recent years luminescence dating has increasingly been applied to date glaciofluvial sediments, but uncertainties about the degree of bleaching of the luminescence signal make dating challenging. Sub-surface luminescence measurements from cobbles from well-bleached environments are able to confirm that the cobbles were well-bleached at deposition. Having this confirmation when studying heterogeneously bleached environments would be a significant advantage.

Bleaching experiments are undertaken to assess if numerical models of bleaching with depth are correct in nature. Measurements confirm that as the length of exposure increases the luminescence signal is reset to greater depths. Cobbles obtained from Orrisdale Head, Isle of Man, show significant sub-surface bleaching, with rock slices to depths of 12 mm into the cobble sub-surface having been completely bleached at deposition. Fading-corrected IRSL50 ages (20.7 $\pm$ 1.3 ka) agree with independent age control at the site. One cobble also appears to show both the advance (26.2 $\pm$ 0.3 ka) and retreat of the Irish Sea Ice Stream. A major advantage of applying luminescence dating to cobbles instead of sand-sized grains is that at depths of >2 mm into the cobble 92% of the dose rate comes from the cobble itself and this makes luminescence ages insensitive to water content.

In further tests of this approach, cobbles from two locations in north Wales show limited sub-surface bleaching, however the IRSL50 ages from the surface slices agree with independent age control. Following the trial at locations with independent age control, cobbles are obtained from a deposit at Bridgwalton which marks the furthest extent of a separate ice lobe which occupied the Cheshire-Shropshire basin. The IRSL50 age (25.3 $\pm$ 1.6 ka) gives the first depositional age for this location and shows that the Last Glacial Maximum (LGM) at this site is synchronous with that observed for the Irish Sea ice stream at the Scilly Isles. Luminescence dating of cobbles has an enormous potential in providing accurate and robust ages for glaciofluvial sediments that are challenging to date.

A copy of the thesis can be given at request to: gej11@aber.ac.uk

Miao Li

Study on thermal activation characteristics of the ESR signal intensity of moraine quartz E_1' center

May 2019
Institute of Tibetan Plateau Research Chinese Academy of Sciences, Beijing, China
Degree: M.Sc.
Supervisor: Chaolu Yi

The quartz E_1' center is a paramagnetic defect center, and the maximum value of the ESR signal intensity of the E_1' center in its thermal activation has been applied for dating of sediments and determination of sediment sources. However, there are still different views on the method for obtaining the maximum value of the thermal activation ESR signal intensity of the E_1' center, such as whether artificial irradiation is needed before heating, whether there is a difference in the optimum thermal activation of temperature and time of the E_1' center, and it needs further study. In addition, there has been no report on the study of moraine provenance by using the ESR signal intensity of the quartz E_1' center at present.

In order to clarify the method of obtaining the maximum value of the thermal activation intensity of the E_1' center and to provide basic experimental data and theoretical references for practical application, the thermal activation characteristics of the ESR signal intensity of moraine quartz E_1' center was studied by using artificial gamma irradiation, thermal annealing and ESR signal measurement. Moreover, in order to provide a simple and fast new method for identifying the provenance of plateau moraines, the provenance of moraines on the west side of the Purog Kangri ice field in the inner Tibet was identified by using the natural signal intensity of the quartz E_1' center, the maximum value of the thermal activation intensity of the E_1' center and the quartz crystallinity index (CI).

The specific conclusions are as follows:

(1) At room temperature and in the range of $\lesssim$2500 Gy of artificial irradiation, the ESR signal intensity of the E_1' center increases with the increase of irradiation dose due to the formation of the counterfeit E_1' center, while the signal intensity of the E_1' center decreases with the increase of irradiation dose likely due to the decay of the real E_1' center caused by the gamma ray irradiation.

(2) The optimal temperature (peak temperature) of thermal activation for the E_1' center ESR signal intensity in the quartz from the moraines collected in the West Kunlun Mountain and the Purog Kangri is approximately 300 °C. When the heating temperature was lower than the peak temperature, the signal intensity of the E_1' center increased with the increase of heating time; otherwise, the E_1' center signal intensity decreased.

(3) At the peak temperature, there was a range of the thermal activation time, (or the optimal activation time range) at which the E_1' center signal intensity reached its maximum value. When the activation time exceeded this range, the ESR signal intensity of the E_1' center decreased.

(4) There is a correlation between the ESR signal intensity of the E_1' center and artificial irradiation dose when the E_1' center is in the growth stage; when the E_1' center decays, it is less correlated with irradiation dose.
(5) The maximum ESR signal intensity of the thermal activation of the E_1' center in the quartz samples both from West Kunlun Mountain and Purog Kangri increased first with the increase of artificial irradiation dose, and then saturated above 400 Gy, indicating that artificial irradiation is needed in order to obtain the maximum ESR signal intensity of the thermal activation of the E_1' center.
(6) The natural signal intensity of the quartz E_1' center, the thermal activation peak intensity of the E_1' center and the quartz crystallinity index (CI) indicate that 73% – 93% of the moraine sediment furthest away from the west side of the Purog Kangri ice field came from the north side and only 7% – 27% from the east side.
(7) The natural signal intensity and the maximum value of the thermal activation ESR signal intensity of the quartz E_1' center and the quartz crystallinity index (CI) can both provide effective guidance for identification of provenance for moraine, and the ESR technology is suitable for the study of the provenance of plateau moraines.

A PDF of this thesis can be downloaded from: Chinese Academy of Sciences Dissertation Database.

Ian del Río

Técnicas de datación por luminiscencia en el norte de Chile: implicación para la evolución tectónica y geomorfológica de la Península de Mejillones durante el Cuaternario
(Luminescence dating in northern Chile: Implications for the Quaternary tectonic and geomorphologic evolution of the Mejillones Peninsula)

May 2019

Departamento de Ciencias Geológicas, Universidad Católica del Norte, Antofagasta, Chile

Degree: Ph.D.
Supervisors: Gabriel González, André Oliveira Sawakuchi

The geomorphology of the Mejillones Peninsula, northern Chile, evidences a Quaternary tectonic uplifting process. Upper plate faults located close to the peninsula show recent activity. However, there is no consensus about the uplift rate of the Mejillones Peninsula in the millennial timescale and numeric ages of uplifted sediments or sediments related to fault activity are scarce. These geochronological data is crucial to establishing the geologic history of the upper plate faults and to improving the understanding on plate tectonics processes in Chile. The main aim of this Ph.D. thesis is to contribute to a better knowledge of the subduction process and upper plate deformation relationship through the quantification of the coastal uplift and the upper plate fault activity in the Mejillones Peninsula for the Late Quaternary applying luminescence dating techniques to quartz and potassium feldspar. To achieve this, 31 sediment samples were collected from four localities: marine-coastal sediments from the Pampa Mejillones, an alluvial deposit associated to the Mejillones Fault, alluvial and eolian deposits associated to the Naguayán Fault and a colluvial deposit associated to the Salar del Carmen Fault. Topographic profiles from the Mejillones Peninsula and the studied faults were obtained by means of a differential GPS. Trenches were excavated in the fault traces for paleoseismic analysis and their fault scarps were modelled with high-resolution 3D techniques.

Optically stimulated luminescence (OSL) signals from quartz and post-infrared infrared stimulated luminescence (pIRIR) signals from K-feldspar were analyzed to determine sediment burial ages. From the comparison between OSL and pIRIR ages, it was concluded that the OSL ages from quartz are largely underestimated. This is attributed to the fact that the quartz OSL signals lack a strong fast OSL component and that predominant medium and slow components show thermal instability. On the other hand, pIRIR signals are close to stability, showing low, though variable, fading rates (0.7 – 6.77%/decade), and bleachable, presenting low residual doses in modern analogues (between 2 and 6 Gy). The alluvial sediments spatially associated with the Mejillones Fault yielded fading-corrected pIRIR ages between 87.4 $\pm$ 6.6 and 163.4 $\pm$ 18.4 ka. For the sediments associated with the Naguayán fault, the fading-corrected pIRIR ages were between 10.4 $\pm$ 1.3 and 44.1 $\pm$ 4.7 ka. The fading-corrected pIRIR ages of the colluvial sediments associated with the Salar del Carmen Fault resulted between 14.7 $\pm$ 1.0 and 131.6 $\pm$ 74.2 ka. For the coastal sediments from the Mejillones Pampa, fading-corrected pIRIR ages were from 70.6 $\pm$ 5.1 to $>$ 330 ka.

From the paleosismological study of the Naguayán and Salar del Carmen Faults, it is concluded that the activity of these faults has been continued during the Late Pleistocene and Holocene. The activity rates of both faults classify them as slow faults, with slip rates of $\sim$ 0.06 m/ka and earthquakes recurrences of 20 ka. Based on stratigraphic references such as colluvial wedges, it was possible to estimate coseismic displacements of up to 2 m, translating into magnitudes of paleoearthquakes of up to Mw7.2. In the specific case of the Naguayán Fault, at least four events could be identified, two of which occurred less than 40 ka ago. According to the pIRIR ages obtained for the studied sediments, Pampa Mejillones has uplifted at rates ranging from 0.25 to 0.5 m/ka between 400 and 100 ka. For the last 70 ka, the pIRIR age obtained in a coastal marine deposit suggests an uplift acceleration to 1.01 m/ka. The activity of the Mejillones Fault, estimated in 0.26 m/ka, partially controls the disposition, formation and preservation of the paleocoastlines, in combination with the variation of relative sea level. Based on these data, an evolution model of the Mejillones Peninsula during the Late Pleistocene is proposed according to which the coastal deposits found in the Pampa Mejillones record coast-

line progradation and retrogradation as a consequence of the combination of tectonic uplift, eustatic sea level variation and upper plate fault activity. An excess in the uplift rate over the subsidence produced by the activity of the Mejillones Fault would elevate the Pampa Mejillones surface, generating the current coastal cliff. Therefore, coastal uplifting process and the upper plate fault activity, especially the potential reactivation of Mejillones and Naguayán faults, must be considered as a potential seismic hazard to the urban and productive infrastructure of Mejillones and industrial complexes located in the Coastal Cordillera.

A PDF of this thesis can be requested from the author at idelrio@alumnos.ucn.cl.

Bibliography

Compiled by Sebastien Huot

From 1st December 2018 to 15th May 2019

Various geological applications

- aeolian

Baldauf, P.E., Burkhart, P.A., Hanson, P.R., Miles, M., Larsen, A., 2019. Chronology of dune development in the White River Badlands, northern Great Plains, USA. Aeolian Research 37, 14-24, http://doi.org/10.1016/j.aeolia.2018.12.004

Barrineau, P., Dobreva, I., Bishop, M.P., Houser, C., Forman, S.L., 2019. Deconstructing aeolian landscapes. CATENA 174, 452-468, http://doi.org/10.1016/j.catena.2018.11.038

Durcan, J.A., Thomas, D.S.G., Gupta, S., Pawar, V., Singh, R.N., Petrie, C.A., 2019. Holocene landscape dynamics in the Ghaggar-Hakra palaeochannel region at the northern edge of the Thar Desert, northwest India. Quaternary International 501, 317-327, http://doi.org/10.1016/j.quaint.2017.10.012

Fulop, E.C.F., Johnson, B.G., Keen-Zebert, A., 2019. A geochronology-supported soil chronosequence for establishing the timing of shoreline parabolic dune stabilization. CATENA 178, 232-243, http://doi.org/10.1016/j.catena.2019.03.018

Johnson, W.C., Halfen, A.F., Spencer, J.Q.G., Hanson, P.R., Mason, J.A., Young, A.R., 2019. Late MIS 3 stabilization of dunes in the eastern Central Great Plains, USA. Aeolian Research 36, 68-81, http://doi.org/10.1016/j.aeolia.2018.12.002

Wang, X., Ma, J., Yi, S., Vandenberghe, J., Dai, Y., Lu, H., 2018. Interaction of fluvial and eolian sedimentation processes, and response to climate change since the last glacial in a semiarid environment along the Yellow River. Quaternary Research 91, 570-583, http://doi.org/10.1017/qua.2018.22

Yan, D., Wünnemann, B., Zhang, Y., Long, H., Stauch, G., Sun, Q., Cao, G., 2018. Response of lake-catchment processes to Holocene climate variability: Evidences from the NE Tibetan Plateau. Quaternary Science Reviews 201, 261-279, http://doi.org/10.1016/j.quascirev.2018.10.017

- alluvial fan

Yu, S.-Y., Du, J., Hou, Z., Shen, J., Colman, S.M., 2019. Late-Quaternary dynamics and palaeoclimatic implications of an alluvial fan-lake system on the southern Alxa Plateau, NW China. Geomorphology 327, 1-13, http://doi.org/10.1016/j.geomorph.2018.10.012

- coastal

Carr, A.S., Bateman, M.D., Cawthra, H.C., Sealy, J., 2019. First evidence for onshore marine isotope stage 3 aeolianite formation on the southern Cape coastline of South Africa. Marine Geology 407, 1-15, http://doi.org/10.1016/j.margeo.2018.10.003

Fruergaard, M., Kirkegaard, L., Østergaard, A.T., Murray, A.S., Andersen, T.J., 2019. Dune ridge progradation resulting from updrift coastal reconfiguration and increased littoral drift. Geomorphology 330, 69-80, http://doi.org/10.1016/j.geomorph.2019.01.008

Makwana, N., Prizomwala, S.P., Chauhan, G., Phartiyal, B., Thakkar, M.G., 2019. Late Holocene palaeo-environmental change in the Banni Plains, Kachchh, Western India. Quaternary International 507, 197-205, http://doi.org/10.1016/j.quaint.2018.11.028

- colluvial

Furbish, D.J., Roering, J.J., Keen-Zebert, A., Almond, P., Doane, T.H., Schumer, R., 2018. Soil Particle Transport and Mixing Near a Hillslope Crest: 2. Cosmogenic Nuclide and Optically Stimulated Luminescence Tracers. Journal of Geophysical Research: Earth Surface 123, 1078-1093, http://doi.org/doi:10.1029/2017JF004316

Kanari, M., Katz, O., Weinberger, R., Porat, N., Marco, S., 2019. Evaluating earthquake-induced rockfall hazard near the Dead Sea Transform. Natural Hazards and Earth System Sciences 19, 889-906, http://doi.org/10.5194/nhess-19-889-2019

Poręba, G., Śnieszko, Z., Moska, P., Mroczek, P., 2019. Deposits of Neolithic water soil erosion in the loess region of the Małopolska Upland (S Poland) – A case study of the settlement micro-region in Bronocice. Quaternary International 502, 45-59, http://doi.org/10.1016/j.quaint.2018.09.018

Poręba, G., Śnieszko, Z., Moska, P., Mroczek, P., Malik, I., 2019. Interpretation of soil erosion in a polish loess area using OSL, 137Cs, 210Pbex, dendrochronology and micromorphology - case study: Biedrzykowice site (s Poland). Geochronometria 46, 57-78, http://doi.org/10.1515/geochr-2015-0109

- earthquake (and fault related)

Hindle, D., Sedov, B., Lindauer, S., Mackey, K., 2019. The Ulakhan fault surface rupture and the seismicity of the Okhotsk–North America plate boundary. Solid Earth 10, 561-580, http://doi.org/10.5194/se-10-561-2019

van Vliet-Lanoë, B., Authemayou, C., Molliex, S., Field, M.H., Frechen, M., Le Roy, P., Perrot, J., Andrieu-Ponel, V., Grégoire, G., Hallégouët, B., 2018. Middle Pleistocene seismically induced clay diapirism in an intraplate zone, western Brittany, France. Quaternary Research 91, 301-324, http://doi.org/10.1017/qua.2018.63

- fluvial

Abotalib, A.Z., Sultan, M., Jimenez, G., Crossey, L., Karlstrom, K., Forman, S., Krishnamurthy, R.V., Elkadiri, R., Polyak, V., 2019. Complexity of Saharan paleoclimate reconstruction and implications for modern human migration. Earth and Planetary Science Letters 508, 74-84, http://doi.org/10.1016/j.epsl.2018.12.015

Armaş, I., Necea, D., Miclăuş, C., 2019. Fluvial terrace formation and controls in the Lower River Danube, SE Romania. Quaternary International 504, 5-23, http://doi.org/10.1016/j.quaint.2018.03.031

Avşin, N., Vandenberghe, J., van Balen, R., Kıyak, N.G., Öztürk, T., 2019. Tectonic and climatic controls on Quaternary fluvial processes and river terrace formation in a Mediterranean setting, the Göksu River, southern Turkey. Quaternary Research 91, 533-547, http://doi.org/10.1017/qua.2018.129

Cunha, P.P., Martins, A.A., Buylaert, J.-P., Murray, A.S., Gouveia, M.P., Font, E., Pereira, T., Figueiredo, S., Ferreira, C., Bridgland, D.R., Yang, P., Stevaux, J.C., Mota, R., 2019. The Lowermost Tejo River Terrace at Foz do Enxarrique, Portugal: A Palaeoenvironmental Archive from c. 60–35 ka and Its Implications for the Last Neanderthals in Westernmost Iberia. Quaternary 2, 3, http://doi.org/10.3390/quat2010003

Durcan, J.A., Thomas, D.S.G., Gupta, S., Pawar, V., Singh, R.N., Petrie, C.A., 2019. Holocene landscape dynamics in the Ghaggar-Hakra palaeochannel region at the northern edge of the Thar Desert, northwest India. Quaternary International 501, 317-327, http://doi.org/10.1016/j.quaint.2017.10.012

Ghosh, R., Srivastava, P., Shukla, U.K., Sehgal, R.K., Singh, I.B., 2019. 100 kyr sedimentary record of Marginal Gangetic Plain: Implications for forebulge tectonics. Palaeogeography, Palaeoclimatology, Palaeoecology 520, 78-95, http://doi.org/10.1016/j.palaeo.2019.01.035

Kothyari, G.C., Shirvalkar, P., Kandregula, R.S., Rawat, Y., Dumka, R.K., Joshi, N., 2019. Holocene tectonic activity along Kachchh Mainland Fault: Impact on late mature Harappan civilization, Kachchh, western India. Quaternary International 507, 274-287, http://doi.org/10.1016/j.quaint.2018.10.032

McCalpin, J.P., Corominas, J., 2019. Postglacial deformation history of sackungen on the northern slope of Pic d'Encampadana, Andorra. Geomorphology 337, 134-150, http://doi.org/10.1016/j.geomorph.2019.04.007

McCool, J.-P., 2019. Carbonates as evidence for groundwater discharge to the Nile River during the Late Pleistocene and Holocene. Geomorphology 331, 4-21, http://doi.org/10.1016/j.geomorph.2018.09.026

Ocakoğlu, F., Akkiraz, M.S., 2019. A Lower Pleistocene to Holocene terrestrial record from the Eskişehir Graben (Central Anatolia): Paleoclimatic and morphotectonic implications. Quaternary International 510, 88-99, http://doi.org/10.1016/j.quaint.2018.12.026

Prizomwala, S.P., Yadav, G., Solanki, T., Das, A., Chauhan, G., Makwana, N., 2019. Style and stages of valley fill aggradation-incision cycles in the Northern Hill Range, Kachchh, Western India. Quaternary International 510, 18-27, http://doi.org/10.1016/j.quaint.2018.11.020

Pupim, F.N., Sawakuchi, A.O., Almeida, R.P., Ribas, C.C., Kern, A.K., Hartmann, G.A., Chiessi, C.M., Tamura, L.N., Mineli, T.D., Savian, J.F., Grohmann, C.H., Bertassoli, D.J., Stern, A.G., Cruz, F.W., Cracraft, J., 2019. Chronology of Terra Firme formation in Amazonian lowlands reveals a dynamic Quaternary landscape. Quaternary Science Reviews 210, 154-163, http://doi.org/10.1016/j.quascirev.2019.03.008

Rossetti, D.d.F., Gribel, R., Cohen, M.C.L., Valeriano, M.d.M., Tatumi, S.H., Yee, M., 2019. The role of Late Pleistocene-Holocene tectono-sedimentary history on the origin of patches of savanna vegetation in the middle Madeira River, southwest of the Amazonian lowlands. Palaeogeography, Palaeoclimatology, Palaeoecology 526, 136-156, http://doi.org/10.1016/j.palaeo.2019.04.017

Sokołowski, R.J., Janowski, Ł., Hrynowiecka, A., Molodkov, A., 2019. Evolution of fluvial system during the Pleistocene warm stage (Marine Isotope Stage 7) – A case study from the Błądzikowo Formation, N Poland. Quaternary International 501, 109-119, http://doi.org/10.1016/j.quaint.2017.09.042

Štor, T., Schaller, M., Merchel, S., Martínek, K., Rittenour, T., Rugel, G., Scharf, A., 2019. Quaternary evolution of the Ploučnice River system (Bohemian Massif) based on fluvial deposits dated with optically stimulated luminescence and in situ produced cosmogenic nuclides. Geomorphology 329, 152-169, http://doi.org/10.1016/j.geomorph.2018.12.019

Vandenberghe, J., Kasse, C., Popov, D., Markovic, S.B., Vandenberghe, D., Bohncke, S., Gabris, G., 2018. Specifying the External Impact on Fluvial Lowland Evolution: The Last Glacial Tisza (Tisa) Catchment in Hungary and Serbia. Quaternary 1, 14, http://doi.org/10.3390/quat1020014

Wang, X., Ma, J., Yi, S., Vandenberghe, J., Dai, Y., Lu, H., 2018. Interaction of fluvial and eolian sedimentation processes, and response to climate change since the last glacial in a semiarid environment along the Yellow River. Quaternary Research 91, 570-583, http://doi.org/10.1017/qua.2018.22

Zieliński, P., Sokołowski, R.J., Jankowski, M., Standzikowski, K., Fedorowicz, S., 2019. The climatic control of sedimentary environment changes during the Weichselian – An example from the Middle Vistula Region (eastern Poland). Quaternary International 501, 120-134, http://doi.org/10.1016/j.quaint.2018.04.036

- glacial and periglacial

Bradwell, T., Small, D., Fabel, D., Smedley, R.K., Clark, C.D., Saher, M.H., Callard, S.L., Chiverrell, R.C., Dove, D., Moreton, S.G., Roberts, D.H., Duller, G.A.T., Ó Cofaigh, C., 2019. Ice-stream demise dynamically conditioned by trough shape and bed strength. Science Advances 5, eaau1380, http://doi.org/10.1126/sciadv.aau1380

García, J.-L., Maldonado, A., de Porras, M.E., Nuevo Delaunay, A., Reyes, O., Ebensperger, C.A., Binnie, S.A., Lüthgens, C., Méndez, C., 2018. Early deglaciation and paleolake history of Río Cisnes Glacier, Patagonian Ice Sheet (44°S). Quaternary Research 91, 194-217, http://doi.org/10.1017/qua.2018.93

Gromig, R., Wagner, B., Wennrich, V., Fedorov, G., Savelieva, L., Lebas, E., Krastel, S., Brill, D., Andreev, A., Subetto, D., Melles, M., 2019. Deglaciation history of Lake Ladoga (northwestern Russia) based on varved sediments. Boreas 48, 330-348, http://doi.org/10.1111/bor.12379

Roberts, D.H., Grimoldi, E., Callard, L., Evans, D.J.A., Clark, C.D., Stewart, H.A., Dove, D., Saher, M., Ó Cofaigh, C., Chiverrell, R.C., Bateman, M.D., Moreton, S.G., Bradwell, T., Fabel, D., Medialdea, A., 2019. The mixed-bed glacial landform imprint of the North Sea Lobe in the western North Sea. Earth Surface Processes and Landforms 44, 1233-1258, http://doi.org/10.1002/esp.4569

Rother, H., Lorenz, S., Börner, A., Kenzler, M., Siermann, N., Fülling, A., Hrynowiecka, A., Forler, D., Kuznetsov, V., Maksimov, F., Starikova, A., 2019. The terrestrial Eemian to late Weichselian sediment record at Beckentin (NE-Germany): First results from lithostratigraphic, palynological and geochronological analyses. Quaternary International 501, 90-108, http://doi.org/10.1016/j.quaint.2017.08.009

Sharma, S., Shukla, A.D., 2018. Factors governing the pattern of glacier advances since the Last Glacial Maxima in the transitional climate zone of the Southern Zanskar Ranges, NW Himalaya. Quaternary Science Reviews 201, 223-240, http://doi.org/10.1016/j.quascirev.2018.10.006

Shulmeister, J., Thackray, G.D., Rittenour, T.M., Fink, D., Patton, N.R., 2019. The timing and nature of the last glacial cycle in New Zealand. Quaternary Science Reviews 206, 1-20, http://doi.org/10.1016/j.quascirev.2018.12.020

Small, D., Smedley, R.K., Chiverrell, R.C., Scourse, J.D., Cofaigh, C.Ó., Duller, G.A.T., McCarron, S., Burke, M.J., Evans, D.J.A., Fabel, D., Gheorghiu, D.M., Thomas, G.S.P., Xu, S., Clark, C.D., 2018. Trough geometry was a greater influence than climate-ocean forcing in regulating retreat of the marine-based Irish-Sea Ice Stream. GSA Bulletin 130, 1981-1999, http://doi.org/10.1130/b31852.1

Zhang, W., Chai, L., Evans, I.S., Liu, L., Li, Y.-p., Qiao, J.-r., Tang, Q.-y., Sun, B., 2019. Geomorphic features of Quaternary glaciation in the Taniantaweng Mountain, on the southeastern Qinghai-Tibet Plateau. Journal of Mountain Science 16, 256-274, http://doi.org/10.1007/s11629-018-4977-3

- lacustrine

Andreev, A.A., Shumilovskikh, L.S., Savelieva, L.A., Gromig, R., Fedorov, G.B., Ludikova, A., Wagner, B., Wennrich, V., Brill, D., Melles, M., 2019. Environmental conditions in northwestern Russia during MIS 5 inferred from the pollen stratigraphy in a sediment core from Lake Ladoga. Boreas 48, 377-386, http://doi.org/10.1111/bor.12382

Cadd, H.R., Tibby, J., Barr, C., Tyler, J., Unger, L., Leng, M.J., Marshall, J.C., McGregor, G., Lewis, R., Arnold, L.J., Lewis, T., Baldock, J., 2018. Development of a southern hemisphere subtropical wetland (Welsby Lagoon, south-east Queensland, Australia) through the last glacial cycle. Quaternary Science Reviews 202, 53-65, http://doi.org/10.1016/j.quascirev.2018.09.010

Jacobs, Z., Li, B., Karkanas, P., Tourloukis, V., Thompson, N., Panagopoulou, E., Harvati, K., 2018. Optical dating of K-feldspar grains from Middle Pleistocene lacustrine sediment at Marathousa 1 (Greece). Quaternary International 497, 170-177, http://doi.org/10.1016/j.quaint.2018.06.029

Roberts, H.M., Bryant, C.L., Huws, D.G., Lamb, H.F., 2018. Generating long chronologies for lacustrine sediments using luminescence dating: a 250,000 year record from Lake Tana, Ethiopia. Quaternary Science Reviews 202, 66-77, http://doi.org/10.1016/j.quascirev.2018.10.037

Viehberg, F.A., Just, J., Dean, J.R., Wagner, B., Franz, S.O., Klasen, N., Kleinen, T., Ludwig, P., Asrat, A., Lamb, H.F., Leng, M.J., Rethemeyer, J., Milodowski, A.E., Claussen, M., Schäbitz, F., 2018. Environmental change during MIS4 and MIS 3 opened corridors in the Horn of Africa for Homo sapiens expansion. Quaternary Science Reviews 202, 139-153, http://doi.org/10.1016/j.quascirev.2018.09.008

Yu, S.-Y., Du, J., Hou, Z., Shen, J., Colman, S.M., 2019. Late-Quaternary dynamics and palaeoclimatic implications of an alluvial fan-lake system on the southern Alxa Plateau, NW China. Geomorphology 327, 1-13, http://doi.org/10.1016/j.geomorph.2018.10.012

- loess

Antoine, P., Lagroix, F., Jordanova, D., Jordanova, N., Lomax, J., Fuchs, M., Debret, M., Rousseau, D.-D., Hatté, C., Gauthier, C., Moine, O., Taylor, S.N., Till, J.L., Coutard, S., 2019. A remarkable Late Saalian (MIS 6) loess (dust) accumulation in the Lower Danube at Harletz (Bulgaria). Quaternary Science Reviews 207, 80-100, http://doi.org/10.1016/j.quascirev.2019.01.005

Bösken, J., Obreht, I., Zeeden, C., Klasen, N., Hambach, U., Sümegi, P., Lehmkuhl, F., 2019. High-resolution paleoclimatic proxy data from the MIS3/2 transition recorded in northeastern Hungarian loess. Quaternary International 502, 95-107, http://doi.org/10.1016/j.quaint.2017.12.008

Fischer, P., Hambach, U., Klasen, N., Schulte, P., Zeeden, C., Steininger, F., Lehmkuhl, F., Gerlach, R., Radtke, U., 2019. Landscape instability at the end of MIS 3 in western Central Europe: evidence from a multi proxy study on a Loess-Palaeosol-Sequence from the eastern Lower Rhine Embayment, Germany. Quaternary International 502, 119-136, http://doi.org/10.1016/j.quaint.2017.09.008

Lomax, J., Fuchs, M., Antoine, P., Rousseau, D.-D., Lagroix, F., Hatté, C., Taylor, S.N., Till, J.L., Debret, M., Moine, O., Jordanova, D., 2019. A luminescence-based chronology for the Harletz loess sequence, Bulgaria. Boreas 48, 179-194, http://doi.org/doi:10.1111/bor.12348

Moska, P., Jary, Z., Adamiec, G., Bluszcz, A., 2019. Chronostratigraphy of a loess-palaeosol sequence in Biały Kościół, Poland using OSL and radiocarbon dating. Quaternary International 502, 4-17, http://doi.org/10.1016/j.quaint.2018.05.024

Moska, P., Jary, Z., Adamiec, G., Bluszcz, A., 2019. High resolution dating of loess profile from Strzyżów (Horodło Plateau-Ridge, Volhynia Upland). Quaternary International 502, 18-29, http://doi.org/10.1016/j.quaint.2018.02.016

Perić, Z., Lagerbäck Adolphi, E., Stevens, T., Újvári, G., Zeeden, C., Buylaert, J.-P., Marković, S.B., Hambach, U., Fischer, P., Schmidt, C., Schulte, P., Huayu, L., Shuangwen, Y., Lehmkuhl, F., Obreht, I., Veres, D., Thiel, C., Frechen, M., Jain, M., Vött, A., Zöller, L., Gavrilov, M.B., 2019. Quartz OSL dating of late quaternary Chinese and Serbian loess: A cross Eurasian comparison of dust mass accumulation rates. Quaternary International 502, 30-44, http://doi.org/10.1016/j.quaint.2018.01.010

Poręba, G., Śnieszko, Z., Moska, P., Mroczek, P., 2019. Deposits of Neolithic water soil erosion in the loess region of the Małopolska Upland (S Poland) – A case study of the settlement micro-region in Bronocice. Quaternary International 502, 45-59, http://doi.org/10.1016/j.quaint.2018.09.018

Wang, L., Jia, J., Xia, D., Liu, H., Gao, F., Duan, Y., Wang, Q., Xie, H., Chen, F., 2019. Climate change in arid central Asia since MIS 2 revealed from a loess sequence in Yili Basin, Xinjiang, China. Quaternary International 502, 258-266, http://doi.org/10.1016/j.quaint.2018.02.032

Zhou, Y., Han, Z., Li, X., Wang, Y., Lv, C., Jiang, M., Yang, Q., Xu, Z., Yi, S., Lu, H., 2018. Sandy Loess Records of Precipitation Changes and Monsoon Migrations in the Hunshandake Sandy Land Since the Last Glacial Maximum. Paleoceanography and Paleoclimatology 33, 945-957, http://doi.org/10.1029/2018pa003339

- marine

De Deckker, P., Arnold, L.J., van der Kaars, S., Bayon, G., Stuut, J.-B.W., Perner, K., Lopes dos Santos, R., Uemura, R., Demuro, M., 2019. Marine Isotope Stage 4 in Australasia: A full glacial culminating 65,000 years ago – Global connections and implications for human dispersal. Quaternary Science Reviews 204, 187-207, http://doi.org/10.1016/j.quascirev.2018.11.017

Kim, J.C., Chang, T.S., Yi, S., 2019. OSL chronology of the Huksan Mud Belt, south-eastern Yellow Sea, and its paleoenvironmental implications. Quaternary International 503, 170-177, http://doi.org/10.1016/j.quaint.2018.12.001

- surface exposure dating

Liritzis, I., Bednarik, R.G., Kumar, G., Polymeris, G., Iliopoulos, I., Xanthopoulou, V., Zacharias, N., Vafiadou, A., Bratitsi, M., 2019. Daraki-Chattan rock art constrained osl chronology and multianalytical techniques: A first pilot investigation. Journal of Cultural Heritage 37, 29-43, http://doi.org/10.1016/j.culher.2018.09.018

Luo, M., Chen, J., Liu, J., Qin, J., Owen, L.A., Han, F., Yang, H., Wang, H., Zhang, B., Yin, J., Li, Y., 2018. A test of rock surface luminescence dating using glaciofluvial boulders from the Chinese Pamir. Radiation Measurements 120, 290-297, http://doi.org/10.1016/j.radmeas.2018.07.017

Meyer, M.C., Gliganic, L.A., Jain, M., Sohbati, R., Schmidmair, D., 2018. Lithological controls on light penetration into rock surfaces – Implications for OSL and IRSL surface exposure dating. Radiation Measurements 120, 298-304, http://doi.org/10.1016/j.radmeas.2018.03.004

Ou, X.J., Roberts, H.M., Duller, G.A.T., Gunn, M.D., Perkins, W.T., 2018. Attenuation of light in different rock types and implications for rock surface luminescence dating. Radiation Measurements 120, 305-311, http://doi.org/10.1016/j.radmeas.2018.06.027

Rades, E.F., Sohbati, R., Lüthgens, C., Jain, M., Murray, A.S., 2018. First luminescence-depth profiles from boulders from moraine deposits: Insights into glaciation chronology and transport dynamics in Malta valley, Austria. Radiation Measurements 120, 281-289, http://doi.org/10.1016/j.radmeas.2018.08.011

- thermochronology

Pagonis, V., Brown, N., 2019. On the unchanging shape of thermoluminescence peaks in preheated feldspars: Implications for temperature sensing and thermochronometry. Radiation Measurements 124, 19-28, http://doi.org/10.1016/j.radmeas.2019.01.021

Yukihara, E.G., Coleman, A.C., Biswas, R.H., Lambert, R., Herman, F., King, G.E., 2018. Thermoluminescence analysis for particle temperature sensing and thermochronometry: Principles and fundamental challenges. Radiation Measurements 120, 274-280, http://doi.org/10.1016/j.radmeas.2018.05.007

Archaeology applications

Alperson-Afil, N., Richter, D., Goren-Inbar, N., 2017. Evaluating the intensity of fire at the Acheulian site of Gesher Benot Ya'aqov—Spatial and thermoluminescence analyses. PLOS ONE 12, e0188091, http://doi.org/10.1371/journal.pone.0188091

Anderson, A., 2019. Was there mid Holocene habitation in Madagascar? A reconsideration of the OSL dates from Lakaton'i Anja. Antiquity 93, 478-487, http://doi.org/10.15184/aqy.2018.161

Demuro, M., Arnold, L.J., Aranburu, A., Sala, N., Arsuaga, J.-L., 2019. New bracketing luminescence ages constrain the Sima de los Huesos hominin fossils (Atapuerca, Spain) to MIS 12. Journal of Human Evolution 131, 76-95, http://doi.org/10.1016/j.jhevol.2018.12.003

Doerschner, N., Fitzsimmons, K.E., Blasco, R., Finlayson, G., Rodríguez-Vidal, J., Rosell, J., Hublin, J.-J., Finlayson, C., 2019. Chronology of the Late Pleistocene archaeological sequence at Vanguard Cave, Gibraltar: Insights from quartz single and multiple grain luminescence dating. Quaternary International 501, 289-302, http://doi.org/10.1016/j.quaint.2018.02.020

Hérisson, D., Airvaux, J., Lenoble, A., Richter, D., Claud, E., Primault, J., 2016. Between the northern and southern regions of Western Europe: The Acheulean site of La Grande Vallée (Colombiers, Vienne, France). Quaternary International 411, 108-131, http://doi.org/10.1016/j.quaint.2015.12.100

Kehl, M., Álvarez-Alonso, D., de Andrés-Herrero, M., Díez-Herrero, A., Klasen, N., Rethemeyer, J., Weniger, G.-C., 2018. The rock shelter Abrigo del Molino (Segovia, Spain) and the timing of the late Middle Paleolithic in Central Iberia. Quaternary Research 90, 180-200, http://doi.org/10.1017/qua.2018.13

Liritzis, I., Bednarik, R.G., Kumar, G., Polymeris, G., Iliopoulos, I., Xanthopoulou, V., Zacharias, N., Vafiadou, A., Bratitsi, M., 2019. Daraki-Chattan rock art constrained osl chronology and multianalytical techniques: A first pilot investigation. Journal of Cultural Heritage 37, 29-43, http://doi.org/10.1016/j.culher.2018.09.018

Liritzis, I., Polymeris, G.S., Vafiadou, A., Sideris, A., Levy, T.E., 2019. Luminescence dating of stone wall, tomb and ceramics of Kastrouli (Phokis, Greece) Late Helladic settlement: Case study. Journal of Cultural Heritage 35, 76-85, http://doi.org/10.1016/j.culher.2018.07.009

Masojć, M., Nassr, A., Kim, J.Y., Krupa-Kurzynowska, J., Sohn, Y.K., Szmit, M., Kim, J.C., Kim, J.S., Choi, H.W., Wieczorek, M., Timmermann, A., 2019. Saharan green corridors and Middle Pleistocene hominin dispersals across the Eastern Desert, Sudan. Journal of Human Evolution 130, 141-150, http://doi.org/10.1016/j.jhevol.2019.01.004

Ocakoğlu, F., Dinçer, B., Akkiraz, M.S., Şahiner, E., Brook, G.A., 2018. Palaeolithic occupation of the Anatolian High Plateau during a cold period: An MIS 6 aged artifact from the Avlamış Valley, Eskişehir, NW Turkey. Geoarchaeology 33, 605-619, http://doi.org/10.1002/gea.21679

Rui, X., Guo, Y.-J., Zhang, J.-F., Hu, Y., Mei, H.-J., Wang, Y.-P., Xie, F., Li, B., 2019. Luminescence chronology of the Palaeolithic–Neolithic transition in the Yujiagou site at the Nihewan Basin, northern China. Journal of Quaternary Science 34, 125-137, http://doi.org/10.1002/jqs.3086

Sanjurjo-Sánchez, J., Montero Fenollós, J.L., Polymeris, G.S., 2018. Technological aspects of Mesopotamian Uruk pottery: estimating firing temperatures using mineralogical methods, thermal analysis and luminescence techniques. Archaeological and Anthropological Sciences 10, 849-864, http://doi.org/10.1007/s12520-016-0409-x

Williams, A.N., Toms, P.S., Marcus, D., Yousif, A., McGuinness, J., O'Sullivan, A., Barry, L., Bryant, T., Wood, J.C., 2019. The first successful application of Optically Stimulated Luminescence dating to a colonial era (<0.25 ka) archaeological site in Australia. Journal of Archaeological Science: Reports 24, 993-1002, http://doi.org/10.1016/j.jasrep.2019.03.020

Williams, T.J., Collins, M.B., Rodrigues, K., Rink, W.J., Velchoff, N., Keen-Zebert, A., Gilmer, A., Frederick, C.D., Ayala, S.J., Prewitt, E.R., 2018. Evidence of an early projectile point technology in North America at the Gault Site, Texas, USA. Science Advances 4, eaar5954, http://doi.org/10.1126/sciadv.aar5954

Various ESR applications

Ahadova, A.S., Mammadov, S.G., Bayramov, M.A., 2019. Spectral Deconvolution of Fossil Tooth Enamel Electron Paramagnetic Resonance Spectrum. World Scientific Research 6, 1-4, http://doi.org/10.20448/

Bi, W., Yi, C., Yang, H., 2018. Quantitative relation between the ESR signal intensities in Ge and E' centers and quartz mass. Radiation Measurements 120, 66-72, http://doi.org/10.1016/j.radmeas.2018.04.007

Gonzales, C.A.B., Yasuda, H., Hirota, S., Miki, K., Saito, A., Taño, J.E., Nagata, Y., 2019. Investigation of the applicability of the ESR nail dosimetry for assessment of accidental exposure in medical facilities. Radiation Measurements 124, 91-97, http://doi.org/10.1016/j.radmeas.2019.03.015

Mashkovtsev, R.I., Pan, Y., 2018. EPR study of new E′ centers in neutron-irradiated α-quartz. EPL (Europhysics Letters) 124, 54001, http://doi.org/10.1209/0295-5075/124/54001

Meriç, N., Aşlar, E., Şahiner, E., Kadioğlu, Y.K., Polymeris, G.S., 2018. Step annealing and fading studies on EPR signals of Durango apatite for various grain size fractions at the edge of the nano-scale; comparison with the corresponding luminescence results. Radiation Measurements 120, 241-246, http://doi.org/10.1016/j.radmeas.2018.05.001

Timar-Gabor, A., 2018. Electron spin resonance characterisation of sedimentary quartz of different grain sizes. Radiation Measurements 120, 59-65, http://doi.org/10.1016/j.radmeas.2018.06.023

Tsukamoto, S., Long, H., Richter, M., Li, Y., King, G.E., He, Z., Yang, L., Zhang, J., Lambert, R., 2018. Quartz natural and laboratory ESR dose response curves: A first attempt from Chinese loess. Radiation Measurements 120, 137-142, http://doi.org/10.1016/j.radmeas.2018.09.008

Zhang, W., Chai, L., Evans, I.S., Liu, L., Li, Y.-p., Qiao, J.-r., Tang, Q.-y., Sun, B., 2019. Geomorphic features of Quaternary glaciation in the Taniantaweng Mountain, on the southeastern Qinghai-Tibet Plateau. Journal of Mountain Science 16, 256-274, http://doi.org/10.1007/s11629-018-4977-3

Basic research

Anechitei-Deacu, V., Timar-Gabor, A., Thomsen, K.J., Buylaert, J.P., Jain, M., Bailey, M., Murray, A.S., 2018. Single and multi-grain OSL investigations in the high dose range using coarse quartz. Radiation Measurements 120, 124-130, http://doi.org/10.1016/j.radmeas.2018.06.008

Ankjærgaard, C., 2019. Exploring multiple-aliquot methods for quartz violet stimulated luminescence dating. Quaternary Geochronology 51, 99-109, http://doi.org/10.1016/j.quageo.2019.02.001

Antohi-Trandafir, O., Timar-Gabor, A., Vulpoi, A., Bălc, R., Longman, J., Veres, D., Simon, S., 2018. Luminescence properties of natural muscovite relevant to optical dating of contaminated quartz samples. Radiation Measurements 109, 1-7, http://doi.org/10.1016/j.radmeas.2017.12.004

Autzen, M., Murray, A.S., Guérin, G., Baly, L., Ankjærgaard, C., Bailey, M., Jain, M., Buylaert, J.P., 2018. Luminescence dosimetry: Does charge imbalance matter? Radiation Measurements 120, 26-32, http://doi.org/10.1016/j.radmeas.2018.08.001

Bailiff, I.K., 2018. An examination of beta dose attenuation effects in coarse grains located in sliced samples. Radiation Measurements 120, 188-194, http://doi.org/10.1016/j.radmeas.2018.07.015

Bi, W., Yi, C., Yang, H., 2018. Quantitative relation between the ESR signal intensities in Ge and E' centers and quartz mass. Radiation Measurements 120, 66-72, http://doi.org/10.1016/j.radmeas.2018.04.007

Bossin, L., Bailiff, I.K., Terry, I., 2018. Phototransferred TL properties of alumina substrates. Radiation Measurements 120, 41-46, http://doi.org/10.1016/j.radmeas.2018.07.018

Bu, M., Murray, A.S., Kook, M., Helsted, L.M., Buylaert, J.-P., Thomsen, K.J., 2018. Characterisation of scintillator-based gamma spectrometers for determination of sample dose rate in OSL dating applications. Radiation Measurements 120, 253-259, http://doi.org/10.1016/j.radmeas.2018.07.003

Buylaert, J.P., Újvári, G., Murray, A.S., Smedley, R.K., Kook, M., 2018. On the relationship between K concentration, grain size and dose in feldspar. Radiation Measurements 120, 181-187, http://doi.org/10.1016/j.radmeas.2018.06.003

Carter, J., Cresswell, A.J., Kinnaird, T.C., Carmichael, L.A., Murphy, S., Sanderson, D.C.W., 2018. Non-Poisson variations in photomultipliers and implications for luminescence dating. Radiation Measurements 120, 267-273, http://doi.org/10.1016/j.radmeas.2018.05.010

Chamberlain, E.L., Wallinga, J., Shen, Z., 2018. Luminescence age modeling of variably-bleached sediment: Model selection and input. Radiation Measurements 120, 221-227, http://doi.org/10.1016/j.radmeas.2018.06.007

Chithambo, M.L., Kalita, J.M., 2018. Optically stimulated luminescence of ultra-high molecular weight polyethylene: A study of dosimetric features. Radiation Measurements 120, 78-82, http://doi.org/10.1016/j.radmeas.2018.06.006

Christophe, C., Philippe, A., Guérin, G., Mercier, N., Guibert, P., 2018. Bayesian approach to OSL dating of poorly bleached sediment samples: Mixture Distribution Models for Dose (MD2). Radiation Measurements 108, 59-73, http://doi.org/10.1016/j.radmeas.2017.10.007

Chruścińska, A., 2019. Advantages and limitations of stimulation with band shape modulation in OSL measurements. Radiation Measurements 124, 63-68, http://doi.org/10.1016/j.radmeas.2019.03.009

Chruścińska, A., Szramowski, A., 2018. Thermally modulated OSL related to the fast component of the OSL signal in quartz. Radiation Measurements 120, 20-25, http://doi.org/10.1016/j.radmeas.2018.05.011

Colarossi, D., Chapot, M.S., Duller, G.A.T., Roberts, H.M., 2018. Testing single aliquot regenerative dose (SAR) protocols for violet stimulated luminescence. Radiation Measurements 120, 104-109, http://doi.org/10.1016/j.radmeas.2018.02.005

Colarossi, D., Duller, G.A.T., Roberts, H.M., 2018. Exploring the behaviour of luminescence signals from feldspars: Implications for the single aliquot regenerative dose protocol. Radiation Measurements 109, 35-44, http://doi.org/10.1016/j.radmeas.2017.07.005

Cresswell, A.J., Carter, J., Sanderson, D.C.W., 2018. Dose rate conversion parameters: Assessment of nuclear data. Radiation Measurements 120, 195-201, http://doi.org/10.1016/j.radmeas.2018.02.007

Cunningham, A.C., Murray, A.S., Armitage, S.J., Autzen, M., 2018. High-precision natural dose rate estimates through beta counting. Radiation Measurements 120, 209-214, http://doi.org/10.1016/j.radmeas.2018.04.008

Dawam, R.R., Chithambo, M.L., 2018. Thermoluminescence of annealed synthetic quartz: The influence of annealing on kinetic parameters and thermal quenching. Radiation Measurements 120, 47-52, http://doi.org/10.1016/j.radmeas.2018.06.004

Discher, M., Mauz, B., Martin, L., Durcan, J.A., King, G.E., Tsakalos, E., Christodoulakis, J., Lang, A., 2018. Calculating or simulating the dose rate? A comparison. Radiation Measurements 120, 202-208, http://doi.org/10.1016/j.radmeas.2018.09.006

Durcan, J.A., 2018. Assessing the reproducibility of quartz OSL lifetime determinations derived using isothermal decay. Radiation Measurements 120, 234-240, http://doi.org/10.1016/j.radmeas.2018.06.020

Folley, D.E., Chithambo, M.L., 2018. Influence of annealing on thermoluminescence of natural quartz: Kinetic analysis and experimental study of apparent inverse thermal quenching. Radiation Measurements 120, 53-58, http://doi.org/10.1016/j.radmeas.2018.04.010

Friedrich, J., Kreutzer, S., Schmidt, C., 2018. Radiofluorescence as a detection tool for quartz luminescence quenching processes. Radiation Measurements 120, 33-40, http://doi.org/10.1016/j.radmeas.2018.03.008

Hansen, V., Murray, A., Thomsen, K., Jain, M., Autzen, M., Buylaert, J.-P., 2018. Towards the origins of over-dispersion in beta source calibration. Radiation Measurements 120, 157-162, http://doi.org/10.1016/j.radmeas.2018.05.014

Heydari, M., Guérin, G., 2018. OSL signal saturation and dose rate variability: Investigating the behaviour of different statistical models. Radiation Measurements 120, 96-103, http://doi.org/10.1016/j.radmeas.2018.05.005

Hunter, P.G., Spooner, N.A., Smith, B.W., 2018. Thermoluminescence emission from quartz at 480 nm as a high-dose radiation marker. Radiation Measurements 120, 143-147, http://doi.org/10.1016/j.radmeas.2018.04.001

Kabacińska, Z., Krzyminiewski, R., Tadyszak, K., Coy, E., 2019. Generation of UV-induced radiation defects in calcite. Quaternary Geochronology 51, 24-42, http://doi.org/10.1016/j.quageo.2019.01.002

Kook, M., Kumar, R., Murray, A.S., Thomsen, K.J., Jain, M., 2018. Instrumentation for the non-destructive optical measurement of trapped electrons in feldspar. Radiation Measurements 120, 247-252, http://doi.org/10.1016/j.radmeas.2018.06.001

Kreutzer, S., Martin, L., Dubernet, S., Mercier, N., 2018. The IR-RF alpha-Efficiency of K-feldspar. Radiation Measurements 120, 148-156, http://doi.org/10.1016/j.radmeas.2018.04.019

Kröninger, K., Mentzel, F., Theinert, R., Walbersloh, J., 2019. A machine learning approach to glow curve analysis. Radiation Measurements 125, 34-39, http://doi.org/10.1016/j.radmeas.2019.02.015

Kumar, R., Kook, M., Murray, A.S., Jain, M., 2018. Towards direct measurement of electrons in metastable states in K-feldspar: Do infrared-photoluminescence and radioluminescence probe the same trap? Radiation Measurements 120, 7-13, http://doi.org/10.1016/j.radmeas.2018.06.018

Lamothe, M., Forget Brisson, L., Hardy, F., 2018. Dose recovery performance in double IRSL/pIRIR SAR protocols. Radiation Measurements 120, 120-123, http://doi.org/10.1016/j.radmeas.2018.05.003

Lawless, J.L., Chen, R., Pagonis, V., 2019. Thermoluminescence governed by the Auger-recombination process. Radiation Measurements 124, 40-47, http://doi.org/10.1016/j.radmeas.2019.03.002

Li, Y., Tsukamoto, S., Long, H., Zhang, J., Yang, L., He, Z., Frechen, M., 2018. Testing the reliability of fading correction methods for feldspar IRSL dating: A comparison between natural and simulated-natural dose response curves. Radiation Measurements 120, 228-233, http://doi.org/10.1016/j.radmeas.2018.06.025

Luo, M., Chen, J., Liu, J., Qin, J., Owen, L.A., Han, F., Yang, H., Wang, H., Zhang, B., Yin, J., Li, Y., 2018. A test of rock surface luminescence dating using glaciofluvial boulders from the Chinese Pamir. Radiation Measurements 120, 290-297, http://doi.org/10.1016/j.radmeas.2018.07.017

Mashkovtsev, R.I., Pan, Y., 2018. EPR study of new E′ centers in neutron-irradiated α-quartz. EPL (Europhysics Letters) 124, 54001, http://doi.org/10.1209/0295-5075/124/54001

Merezhnikov, A.S., Nikiforov, S.V., Pagonis, V., 2019. Simulation of TL kinetics in complex trap cluster systems: Some new approaches. Radiation Measurements 125, 78-84, http://doi.org/10.1016/j.radmeas.2019.04.021

Meriç, N., Aşlar, E., Şahiner, E., Kadioğlu, Y.K., Polymeris, G.S., 2018. Step annealing and fading studies on EPR signals of Durango apatite for various grain size fractions at the edge of the nano-scale; comparison with the corresponding luminescence results. Radiation Measurements 120, 241-246, http://doi.org/10.1016/j.radmeas.2018.05.001

Meyer, M.C., Gliganic, L.A., Jain, M., Sohbati, R., Schmidmair, D., 2018. Lithological controls on light penetration into rock surfaces – Implications for OSL and IRSL surface exposure dating. Radiation Measurements 120, 298-304, http://doi.org/10.1016/j.radmeas.2018.03.004

Murari, M.K., Kreutzer, S., Fuchs, M., 2018. Further investigations on IR-RF: Dose recovery and correction. Radiation Measurements 120, 110-119, http://doi.org/10.1016/j.radmeas.2018.04.017

Murray, A.S., Helsted, L.M., Autzen, M., Jain, M., Buylaert, J.P., 2018. Measurement of natural radioactivity: Calibration and performance of a high-resolution gamma spectrometry facility. Radiation Measurements 120, 215-220, http://doi.org/10.1016/j.radmeas.2018.04.006

Nyirenda, A.N., Chithambo, M.L., 2018. Spectral study of radioluminescence in carbon-doped aluminium oxide. Radiation Measurements 120, 89-95, http://doi.org/10.1016/j.radmeas.2018.06.026

Ou, X.J., Roberts, H.M., Duller, G.A.T., Gunn, M.D., Perkins, W.T., 2018. Attenuation of light in different rock types and implications for rock surface luminescence dating. Radiation Measurements 120, 305-311, http://doi.org/10.1016/j.radmeas.2018.06.027

Pagonis, V., Brown, N., 2019. On the unchanging shape of thermoluminescence peaks in preheated feldspars: Implications for temperature sensing and thermochronometry. Radiation Measurements 124, 19-28, http://doi.org/10.1016/j.radmeas.2019.01.021

Pagonis, V., Friedrich, J., Discher, M., Müller-Kirschbaum, A., Schlosser, V., Kreutzer, S., Chen, R., Schmidt, C., 2019. Excited state luminescence signals from a random distribution of defects: A new Monte Carlo simulation approach for feldspar. Journal of Luminescence 207, 266-272, http://doi.org/10.1016/j.jlumin.2018.11.024

Palczewski, P., Chruścińska, A., 2018. Band shape modulation optically stimulated luminescence (BSM-OSL) - Simulations and first experiments. Radiation Measurements 120, 14-19, http://doi.org/10.1016/j.radmeas.2018.06.019

Palczewski, P., Chruścińska, A., 2019. Different components of the quartz OSL signal resolved by the TM-OSL method. Radiation Measurements 121, 32-36, http://doi.org/10.1016/j.radmeas.2018.12.005

Pandey, A., Chithambo, M.L., 2018. Thermoluminescence of the persistent-luminescence phosphor, BaAl2O4; A stuffed tridymite. Radiation Measurements 120, 73-77, http://doi.org/10.1016/j.radmeas.2018.01.004

Polymeris, G.S., Şahiner, E., Kadioğlu, Y.K., Meriç, N., 2018. Properties of quartz TA – OSL signal with a peculiar decay shape for SAR TA – OSL applications. Radiation Measurements 120, 176-180, http://doi.org/10.1016/j.radmeas.2018.04.002

Qin, J., Chen, J., Li, Y., Zhou, L., 2018. Initial sensitivity change of K-feldspar pIRIR signals due to uncompensated decrease in electron trapping probability: Evidence from radiofluorescence measurements. Radiation Measurements 120, 131-136, http://doi.org/10.1016/j.radmeas.2018.06.017

Qiu, Z., Song, H., Hu, C., Wignall, P.B., Song, H., 2019. Carbonate thermoluminescence and its implication for marine productivity change during the Permian-Triassic transition. Palaeogeography, Palaeoclimatology, Palaeoecology 526, 72-79, http://doi.org/10.1016/j.palaeo.2019.04.021

Rades, E.F., Sohbati, R., Lüthgens, C., Jain, M., Murray, A.S., 2018. First luminescence-depth profiles from boulders from moraine deposits: Insights into glaciation chronology and transport dynamics in Malta valley, Austria. Radiation Measurements 120, 281-289, http://doi.org/10.1016/j.radmeas.2018.08.011

Riedesel, S., King, G.E., Prasad, A.K., Kumar, R., Finch, A.A., Jain, M., 2019. Optical determination of the width of the band-tail states, and the excited and ground state energies of the principal dosimetric trap in feldspar. Radiation Measurements 125, 40-51, http://doi.org/10.1016/j.radmeas.2018.08.019

Roberts, H.M., Duller, G.A.T., Gunn, M., Cousins, C.R., Cross, R.E., Langstaff, D., 2018. Strategies for equivalent dose determination without heating, suitable for portable luminescence readers. Radiation Measurements 120, 170-175, http://doi.org/10.1016/j.radmeas.2018.04.018

Sadri, L., Mohammadi, K., Setayeshi, S., Khorasani, M.H., 2019. The two-level version of semi-localized transitions (SLT) model for thermoluminescence dosimeter. Radiation Measurements 123, 44-53, http://doi.org/10.1016/j.radmeas.2019.02.006

Şahiner, E., Erturaç, M.K., Polymeris, G.S., Meriç, N., 2018. Methodological studies on integration time interval's selection for the luminescence ages using quartz and feldspar minerals; sediments collected from Sakarya, Turkey. Radiation Measurements 120, 163-169, http://doi.org/10.1016/j.radmeas.2018.06.024

Thomas, S., Chithambo, M.L., 2018. Characteristics of the thermoluminescence of Sm3+-doped P2O5-K2O-MgO-Al2O3-ZnF2 glass. Radiation Measurements 120, 83-88, http://doi.org/10.1016/j.radmeas.2018.06.005

Thomsen, K.J., Kook, M., Murray, A.S., Jain, M., 2018. Resolving luminescence in spatial and compositional domains. Radiation Measurements 120, 260-266, http://doi.org/10.1016/j.radmeas.2018.06.002

Timar-Gabor, A., 2018. Electron spin resonance characterisation of sedimentary quartz of different grain sizes. Radiation Measurements 120, 59-65, http://doi.org/10.1016/j.radmeas.2018.06.023

Tsukamoto, S., Long, H., Richter, M., Li, Y., King, G.E., He, Z., Yang, L., Zhang, J., Lambert, R., 2018. Quartz natural and laboratory ESR dose response curves: A first attempt from Chinese loess. Radiation Measurements 120, 137-142, http://doi.org/10.1016/j.radmeas.2018.09.008

Williams, O.M., Spooner, N.A., 2018. Defect pair mechanism for quartz intermediate temperature thermoluminescence bands. Radiation Measurements 108, 41-44, http://doi.org/10.1016/j.radmeas.2017.11.005

Yukihara, E.G., 2019. Observation of strong thermally transferred optically stimulated luminescence (TT-OSL) in BeO. Radiation Measurements 121, 103-108, http://doi.org/10.1016/j.radmeas.2018.12.014

Yukihara, E.G., Coleman, A.C., Biswas, R.H., Lambert, R., Herman, F., King, G.E., 2018. Thermoluminescence analysis for particle temperature sensing and thermochronometry: Principles and fundamental challenges. Radiation Measurements 120, 274-280, http://doi.org/10.1016/j.radmeas.2018.05.007

Dose rate issues

Bailiff, I.K., 2018. An examination of beta dose attenuation effects in coarse grains located in sliced samples. Radiation Measurements 120, 188-194, http://doi.org/10.1016/j.radmeas.2018.07.015

Bu, M., Murray, A.S., Kook, M., Helsted, L.M., Buylaert, J.-P., Thomsen, K.J., 2018. Characterisation of scintillator-based gamma spectrometers for determination of sample dose rate in OSL dating applications. Radiation Measurements 120, 253-259, http://doi.org/10.1016/j.radmeas.2018.07.003

Buylaert, J.P., Újvári, G., Murray, A.S., Smedley, R.K., Kook, M., 2018. On the relationship between K concentration, grain size and dose in feldspar. Radiation Measurements 120, 181-187, http://doi.org/10.1016/j.radmeas.2018.06.003

Cresswell, A.J., Carter, J., Sanderson, D.C.W., 2018. Dose rate conversion parameters: Assessment of nuclear data. Radiation Measurements 120, 195-201, http://doi.org/10.1016/j.radmeas.2018.02.007

Cunningham, A.C., Murray, A.S., Armitage, S.J., Autzen, M., 2018. High-precision natural dose rate estimates through beta counting. Radiation Measurements 120, 209-214, http://doi.org/10.1016/j.radmeas.2018.04.008

Discher, M., Mauz, B., Martin, L., Durcan, J.A., King, G.E., Tsakalos, E., Christodoulakis, J., Lang, A., 2018. Calculating or simulating the dose rate? A comparison. Radiation Measurements 120, 202-208, http://doi.org/10.1016/j.radmeas.2018.09.006

Liritzis, I., Bednarik, R.G., Kumar, G., Polymeris, G., Iliopoulos, I., Xanthopoulou, V., Zacharias, N., Vafiadou, A., Bratitsi, M., 2019. Daraki-Chattan rock art constrained osl chronology and multianalytical techniques: A first pilot investigation. Journal of Cultural Heritage 37, 29-43, http://doi.org/10.1016/j.culher.2018.09.018

Murray, A.S., Helsted, L.M., Autzen, M., Jain, M., Buylaert, J.P., 2018. Measurement of natural radioactivity: Calibration and performance of a high-resolution gamma spectrometry facility. Radiation Measurements 120, 215-220, http://doi.org/10.1016/j.radmeas.2018.04.006

Dosimetry

Autzen, M., Murray, A.S., Guérin, G., Baly, L., Ankjærgaard, C., Bailey, M., Jain, M., Buylaert, J.P., 2018. Luminescence dosimetry: Does charge imbalance matter? Radiation Measurements 120, 26-32, http://doi.org/10.1016/j.radmeas.2018.08.001

Bilski, P., 2018. Thermoluminescent Dosimetry of Cosmic Radiation in Space, in: Chen, R., Pagonis, V. (Eds.), Advances in Physics and Applications of Optically and Thermally Stimulated Luminescence. World Scientific (Europe), pp. 285-317, http://doi.org/10.1142/9781786345790_0008

Chithambo, M.L., Kalita, J.M., 2018. Optically stimulated luminescence of ultra-high molecular weight polyethylene: A study of dosimetric features. Radiation Measurements 120, 78-82, http://doi.org/10.1016/j.radmeas.2018.06.006

Gonzales, C.A.B., Yasuda, H., Hirota, S., Miki, K., Saito, A., Taño, J.E., Nagata, Y., 2019. Investigation of the applicability of the ESR nail dosimetry for assessment of accidental exposure in medical facilities. Radiation Measurements 124, 91-97, http://doi.org/10.1016/j.radmeas.2019.03.015

Kim, H., Kim, M.C., Lee, J., Chang, I., Lee, S.K., Kim, J.-L., 2019. Thermoluminescence of AMOLED substrate glasses in recent mobile phones for retrospective dosimetry. Radiation Measurements 122, 53-56, http://doi.org/10.1016/j.radmeas.2019.01.004

McKeever, S.W.S., Sholom, S., 2018. Luminescence Measurements for Retrospective Dosimetry, in: Chen, R., Pagonis, V. (Eds.), Advances in Physics and Applications of Optically and Thermally Stimulated Luminescence. World Scientific (Europe), pp. 319-362, http://doi.org/10.1142/9781786345790_0009

Nikiforov, S.V., Lushchik, A., Nagirnyi, V., Romet, I., Ponomareva, A.I., Ananchenko, D.V., Moiseykin, E.V., 2019. Validation of the model of TSL isothermal decay in dosimetric α-Al2O3 crystals. Radiation Measurements 122, 29-33, http://doi.org/10.1016/j.radmeas.2019.01.009

Nyirenda, A.N., Chithambo, M.L., 2018. Spectral study of radioluminescence in carbon-doped aluminium oxide. Radiation Measurements 120, 89-95, http://doi.org/10.1016/j.radmeas.2018.06.026

Pandey, A., Chithambo, M.L., 2018. Thermoluminescence of the persistent-luminescence phosphor, BaAl2O4; A stuffed tridymite. Radiation Measurements 120, 73-77, http://doi.org/10.1016/j.radmeas.2018.01.004

Sfampa, I.K., Malletzidou, L., Pandoleon, P., Kitis, G., 2019. Thermoluminescence measurements of in-vitro and in-vivo aged porcelain. Radiation Measurements 125, 7-14, http://doi.org/10.1016/j.radmeas.2019.04.017

Thomas, S., Chithambo, M.L., 2018. Characteristics of the thermoluminescence of Sm3+-doped P2O5-K2O-MgO-Al2O3-ZnF2 glass. Radiation Measurements 120, 83-88, http://doi.org/10.1016/j.radmeas.2018.06.005

Wahib, N.b., Khandaker, M.U., Aqilah binti Mohamad Ramli, N., Sani, S.F.A., Bradley, D.A., 2019. Commercial kitchenware glass as a potential thermoluminescent media for retrospective dosimetry. Applied Radiation and Isotopes 148, 218-224, http://doi.org/10.1016/j.apradiso.2019.04.001

Yukihara, E.G., 2019. Observation of strong thermally transferred optically stimulated luminescence (TT-OSL) in BeO. Radiation Measurements 121, 103-108, http://doi.org/10.1016/j.radmeas.2018.12.014

Beyond quartz and K-feldspar: non-traditional minerals

- calcite

Kabacińska, Z., Krzyminiewski, R., Tadyszak, K., Coy, E., 2019. Generation of UV-induced radiation defects in calcite. Quaternary Geochronology 51, 24-42, http://doi.org/10.1016/j.quageo.2019.01.002

Qiu, Z., Song, H., Hu, C., Wignall, P.B., Song, H., 2019. Carbonate thermoluminescence and its implication for marine productivity change during the Permian-Triassic transition. Palaeogeography, Palaeoclimatology, Palaeoecology 526, 72-79, http://doi.org/10.1016/j.palaeo.2019.04.021

- flint

Alperson-Afil, N., Richter, D., Goren-Inbar, N., 2017. Evaluating the intensity of fire at the Acheulian site of Gesher Benot Ya'aqov—Spatial and thermoluminescence analyses. PLOS ONE 12, e0188091, http://doi.org/10.1371/journal.pone.0188091

Hérisson, D., Airvaux, J., Lenoble, A., Richter, D., Claud, E., Primault, J., 2016. Between the northern and southern regions of Western Europe: The Acheulean site of La Grande Vallée (Colombiers, Vienne, France). Quaternary International 411, 108-131, http://doi.org/10.1016/j.quaint.2015.12.100

- muscovite

Antohi-Trandafir, O., Timar-Gabor, A., Vulpoi, A., Bălc, R., Longman, J., Veres, D., Simon, S., 2018. Luminescence properties of natural muscovite relevant to optical dating of contaminated quartz samples. Radiation Measurements 109, 1-7, http://doi.org/10.1016/j.radmeas.2017.12.004

Instruments

Bu, M., Murray, A.S., Kook, M., Helsted, L.M., Buylaert, J.-P., Thomsen, K.J., 2018. Characterisation of scintillator-based gamma spectrometers for determination of sample dose rate in OSL dating applications. Radiation Measurements 120, 253-259, http://doi.org/10.1016/j.radmeas.2018.07.003

Carter, J., Cresswell, A.J., Kinnaird, T.C., Carmichael, L.A., Murphy, S., Sanderson, D.C.W., 2018. Non-Poisson variations in photomultipliers and implications for luminescence dating. Radiation Measurements 120, 267-273, http://doi.org/10.1016/j.radmeas.2018.05.010

Discher, M., Dornich, K., Richter, A., Mauz, B., Lang, A., 2019. Extending the measurement temperature range in a fully automated luminescence reader to −50 °C. Radiation Measurements 124, 13-18, http://doi.org/10.1016/j.radmeas.2019.02.017

Kook, M., Kumar, R., Murray, A.S., Thomsen, K.J., Jain, M., 2018. Instrumentation for the non-destructive optical measurement of trapped electrons in feldspar. Radiation Measurements 120, 247-252, http://doi.org/10.1016/j.radmeas.2018.06.001

Murray, A.S., Helsted, L.M., Autzen, M., Jain, M., Buylaert, J.P., 2018. Measurement of natural radioactivity: Calibration and performance of a high-resolution gamma spectrometry facility. Radiation Measurements 120, 215-220, http://doi.org/10.1016/j.radmeas.2018.04.006

Thomsen, K.J., Kook, M., Murray, A.S., Jain, M., 2018. Resolving luminescence in spatial and compositional domains. Radiation Measurements 120, 260-266, http://doi.org/10.1016/j.radmeas.2018.06.002

- portable instruments

Roberts, H.M., Duller, G.A.T., Gunn, M., Cousins, C.R., Cross, R.E., Langstaff, D., 2018. Strategies for equivalent dose determination without heating, suitable for portable luminescence readers. Radiation Measurements 120, 170-175, http://doi.org/10.1016/j.radmeas.2018.04.018

Rother, H., Lorenz, S., Börner, A., Kenzler, M., Siermann, N., Fülling, A., Hrynowiecka, A., Forler, D., Kuznetsov, V., Maksimov, F., Starikova, A., 2019. The terrestrial Eemian to late Weichselian sediment record at Beckentin (NE-Germany): First results from lithostratigraphic, palynological and geochronological analyses. Quaternary International 501, 90-108, http://doi.org/10.1016/j.quaint.2017.08.009

Review

Bilski, P., 2018. Thermoluminescent Dosimetry of Cosmic Radiation in Space, in: Chen, R., Pagonis, V. (Eds.), Advances in Physics and Applications of Optically and Thermally Stimulated Luminescence. World Scientific (Europe), pp. 285-317, http://doi.org/10.1142/9781786345790_0008

Chen, R., 2018. Recent Advances in the Theory of Thermoluminescence and Optically Stimulated Luminescence; Delocalized Transitions, in: Chen, R., Pagonis, V. (Eds.), Advances in Physics and Applications of Optically and Thermally Stimulated Luminescence. World Scientific (Europe), pp. 1-36, http://doi.org/10.1142/9781786345790_0001

Chen, R., Pagonis, V., 2019. Advances in Physics and Applications of Optically and Thermally Stimulated Luminescence. World Scientific, http://doi.org/10.1142/q0172

Chithambo, M.L., 2018. An introduction to time-resolved optically stimulated luminescence. Morgan & Claypool Publishers, http://doi.org/10.1088/2053-2571/aae5da

Chithambo, M.L., 2018. Time-resolved Luminescence: Progress in Development of Theory and Analytical Methods, in: Chen, R., Pagonis, V. (Eds.), Advances in Physics and Applications of Optically and Thermally Stimulated Luminescence. World Scientific (Europe), pp. 243-284, http://doi.org/10.1142/9781786345790_0007

Chruścińska, A., 2018. Recent Experiments and Theory of OSL, in: Chen, R., Pagonis, V. (Eds.), Advances in Physics and Applications of Optically and Thermally Stimulated Luminescence. World Scientific (Europe), pp. 205-241, http://doi.org/10.1142/9781786345790_0006

DeWerd, L.A., Hammer, C., Kry, S., 2018. Medical Applications of Luminescent Materials, in: Chen, R., Pagonis, V. (Eds.), Advances in Physics and Applications of Optically and Thermally Stimulated Luminescence. World Scientific (Europe), pp. 439-479, http://doi.org/10.1142/9781786345790_0012

Guralnik, B., Sohbati, R., 2018. Fundamentals of Luminescence Photo- and Thermochronometry, in: Chen, R., Pagonis, V. (Eds.), Advances in Physics and Applications of Optically and Thermally Stimulated Luminescence. World Scientific (Europe), pp. 399-437, http://doi.org/10.1142/9781786345790_0011

Horowitz, Y.S., Oster, L., Eliyahu, I., 2018. Modeling the Effects of Ionization Density in Thermoluminescence Mechanisms and Dosimetry, in: Chen, R., Pagonis, V. (Eds.), Advances in Physics and Applications of Optically and Thermally Stimulated Luminescence. World Scientific (Europe), pp. 83-129, http://doi.org/10.1142/9781786345790_0003

Li, S.-H., Li, B., 2018. TL/OSL Dating, in: Chen, R., Pagonis, V. (Eds.), Advances in Physics and Applications of Optically and Thermally Stimulated Luminescence. World Scientific (Europe), pp. 363-398, http://doi.org/10.1142/9781786345790_0010

Martini, M., Fasoli, M., 2018. Luminescence and Defects in Quartz, in: Chen, R., Pagonis, V. (Eds.), Advances in Physics and Applications of Optically and Thermally Stimulated Luminescence. World Scientific (Europe), pp. 173-204, http://doi.org/10.1142/9781786345790_0005

McKeever, S.W.S., Sholom, S., 2018. Luminescence Measurements for Retrospective Dosimetry, in: Chen, R., Pagonis, V. (Eds.), Advances in Physics and Applications of Optically and Thermally Stimulated Luminescence. World Scientific (Europe), pp. 319-362, http://doi.org/10.1142/9781786345790_0009

Pagonis, V., 2018. Recent Advances in the Theory of Quantum Tunneling for Luminescence Phenomena, in: Chen, R., Pagonis, V. (Eds.), Advances in Physics and Applications of Optically and Thermally Stimulated Luminescence. World Scientific (Europe), pp. 37-81, http://doi.org/10.1142/9781786345790_0002

Polymeris, G.S., Kitis, G., 2018. Thermally Assisted Optically Stimulated Luminescence (TA – OSL), in: Chen, R., Pagonis, V. (Eds.), Advances in Physics and Applications of Optically and Thermally Stimulated Luminescence. World Scientific (Europe), pp. 131-171, http://doi.org/10.1142/9781786345790_0004

Conference Announcements: DLED 2019

DLED2019: German Luminescence and Electron Spin Resonance Meeting

This year's DLED will be hosted by Kathryn Fitzsimmons, Aditi Dave and Zoran Perić of the Max Planck Institute for Chemistry in Mainz (https://www.mpic.de/forschung/weitere-forschungsgruppen/gruppe-fitzsimmons.html). It will take place ***8-10 November*** in the town of ***Bingen***, at the confluence of the Rhine and Nahe rivers and an easy hour or so by train north of Frankfurt Airport.

The German Luminescence and Electron Spin Resonance (DLED) meeting is an annual meeting, usually held in Germany or one of its surrounding countries. The meeting allows luminescence and electron spin resonance dating experts from Central Europe to come together to present the latest technical developments and research results, as well as to network. Following the loose tradition of new laboratories hosting the meeting, our Group from Mainz is pleased to welcome you to the southern Rhineland.

The meeting will be held at the Jugendherberge Bingen (https://www.diejugendherbergen.de/jugendherbergen/bingen/portrait/?gclid=EAIaIQobChMIqqbK05yq4gIVFOd3Ch131QheEAAYASAAEgJMJPD_BwE). Registration will be kept low and in keeping with previous DLEDs, will include room and board in shared accommodation at the hostel. Private rooms are available in nearby hotels in town (please contact the organisers for details). The situation of Bingen at the head of the Rhine Gorge, surrounded by forest, offers pleasant opportunities for our Saturday afternoon bushwalk.

Both poster and oral presentations are welcomed; poster presenters will have the opportunity to introduce their topic to the conference audience in two slides in advance of the poster session.

Please contact Kathryn Fitzsimmons (k.fitzsimmons@mpic.de), Aditi Dave (a.dave@mpic.de) and Zoran Perić (z.peric@mpic.de) for details.
We look forward to welcoming you to Bingen!

Conference Announcements: 7th HSA Symposium

7th Symposium on Archaeometry of the Hellenic Society for Archaeometry

9-12 October 2019
Athens, Greece

Following its preliminary declaration, the Board of the Hellenic Society for Archaeometry (HSA) announces the organization of the 7th Symposium on Archaeometry which will be held at the Byzantine and Christian Museum, Athens. The Symposium responds to the long-standing and steadily increasing interest of archaeologists, historians, anthropologists, palaeo-environmental scientists and other specialists of similar directions to collaborate with specialized researchers from the fields of science on issues related to cultural heritage. The forthcoming Symposium is a continuation of the six (6) previous relevant events that were held successfully by the HSA in the past, and is expected to stand as breeding ground for scientific enquiry, dissemination of new knowledge, dialogue between specialists coming from various disciplines, and for training.

Thematic units

- Dating and palaeo-environment
- Geophysical prospection
- Ceramic and vitreous materials
- Ancient and prehistoric metallurgy
- Lithics, with an emphasis on marbles, plasters and pigments
- Biomaterials – bioarchaeology
- Special thematic session on archaeoseismology, geoarchaeology and on issues of precision in absolute dating

Important dates and registration

- **Monday, July 1st, 2019:** Abstract submission deadline
- **Wednesday, July 31st, 2019:** Notification to participants upon acceptance
- **Until, Friday, August 30th, 2019:** Early registration: 80 € - Students: 50€. After the 30th of August: Late registration: 100 € and 80 € respectively.
- **Wednesday, October 9th, 2019:** Symposium commencing.
- **Friday, October 11th, 2019:** Symposium's Dinner, Award ceremony, Honorary distinctions.

Website: http://www.archaeometry.org.gr/
Conference email: archaeometry.org.gr@gmail.com

Organising committee

Y. Bassiakos, Y. Facorellis, E. Filippaki, A. Oikonomou, M. Papageorgiou, P. Loukopoulou, G. Theodorou

Conference Announcements: UK LED 2019

UK Luminescence and ESR Meeting 2019 in Denmark

Technical University of Denmark

This is the second announcement for the 2019 UK Luminescence and ESR meeting in Denmark (UKLUM2019DK). The meeting will be hosted by the Luminescence Physics group at The Centre for Nuclear Technologies, Technical University of Denmark, from 26th-28th August 2019 on the Risø Campus, Roskilde, in collaboration with Aarhus University. UKLUM2019DK will provide an informal forum for discussion of luminescence and electron spin resonance research, with an emphasis on recent developments, ongoing research and student projects. There will be ample place for posters, and both oral and poster presentations are encouraged. We look forward to a full, interesting and varied programme.

If you have already registered an interest but have not received a confirmation mail from us, please resend your message to UKLUM2019.in.DK@nutech.dtu.dk; there have been difficulties with the email link on the webpage.

This will be a no frills meeting in order to keep costs down. Registration is 90 EUR for professionals and 60 EUR for students. This covers two and a half days of presentations, lunch, tea breaks and an icebreaker. There is an optional conference dinner to be held on Tuesday August 27th (45 EUR per person) to be held at the Risø Campus. This will take the form of a buffet with a wide variety of options (including vegetarian) and there will be a cheap honesty bar open during and after the dinner.

There will also be a workshop on Rock Surface Dating to be held at Risø Campus on Sunday August 25th (20 EUR).

Abstract deadline is June 30th, and online registration will be open from May 27th until July 15th. We will update the webpage with a list of possible accommodation and prices, but we encourage anyone intending to attend the conference to book accommodation as soon as possible; Roskilde is a popular tourist destination and budget summer/autumn accommodation is booked up very early.

Further information will be available on https://www.tilmeld.dk/UKLUM19

Please forward this circular to anyone who might be interested and if you would like to be taken off the mailing list please write to UKLUM2019.in.DK@nutech.dtu.dk

We look forward to welcoming you to Risø.

Announcements: Invitation to contribute to Special Issue

I am serving as a Guest Editor for the Special Issue "Methods in Dating and Other Applications using Luminescence" in Open Access journal MPs (ISSN 2409-9279). Based on your extensive experience in this field, we would like to invite you to submit a manuscript in this Special Issue (i.e., Protocols, Benchmarks, Technical Notes, Letters, Reviews or Comments).

The submission deadline is 1 August 2019. You may send your manuscript now or up until the deadline. Submitted papers should not be under consideration for publication elsewhere. We also encourage authors to send a short abstract or tentative title to us first (elsie.zhao@mdpi.com or jimf@uw.edu). For further information, please follow this link: https://www.mdpi.com/journal/mps/special_issues/MDOAL

Methods and Protocols is fully open access. Open access (unlimited and free access by readers) increases publicity and promotes more frequent citations, as indicated by several studies. Open access is supported by the authors and their institutes. No Article Processing Charges (APC) apply for well-prepared manuscripts.

For further details on the submission process, please see the instructions for authors at the journal website (http://www.mdpi.com/journal/mps/instructions).

We hope that this is of interest to you and look forward to hearing from you soon.

James K. Feathers
University of Washington

Ancient TL

ISSN 0735-1348

Aims and Scope

Ancient TL is a journal devoted to Luminescence dating, Electron Spin Resonance (ESR) dating, and related techniques. It aims to publish papers dealing with experimental and theoretical results in this field, with a minimum of delay between submission and publication. Ancient TL also publishes a current bibliography, thesis abstracts, letters, and miscellaneous information, e.g., announcements for meetings.

Frequency

Two issues per annum in June and December

Submission of articles to Ancient TL

Ancient TL has a reviewing system in which direct dialogue is encouraged between reviewers and authors. For instructions to authors and information on how to submit to Ancient TL, please visit the website at:
http://ancienttl.org/TOC1.htm

Journal Enquiries

For enquiries please contact the editor:
Regina DeWitt, Department of Physics, East Carolina University, Howell Science Complex, 1000 E. 5th Street, Greenville, NC 27858, USA; Tel: +252-328-4980; Fax: +252-328-0753 (dewittr@ecu.edu)

Subscriptions to Ancient TL

Ancient TL Vol. 32 No.2 December 2014 was the last issue to be published in print. Past and current issues are available for download free of charge from the Ancient TL website:
http://ancienttl.org/TOC4.htm